Regulation of Expression and Physiological Function of Type VI 3β-Hydroxysteroid Dehydrogenase Isozyme Hsd3b6
（VI 型 3β−水酸化ステロイド脱水素酵素 Hsd3b6 の発現制御と生理機能の解明）

2018

鑓水 大介

Contents

Prolegomenon

The enzyme 3β-hydroxysteroid dehydrogenase/isomerase (3β-HSD) is essential for the biosynthesis of all active steroid hormones, such as those secreted from the adrenal gland, testis, ovary, skin, and placenta. The 3β-HSD enzymes exist in multiple isoforms in humans and rodents with different tissue specificity. The mouse has two isoforms in the adrenal: one (Hsd3b1) is ubiquitous in the cortex, but the other (Hsd3b6) is specific to the zona glomerulosa (ZG), where aldosterone is produced [1]. Both genes are evolutionally conserved in humans, with the genes named *HSD3B1* and *HSD3B2* being a candidate counterpart of the mouse *Hsd3b6* and *Hsd3b1*, respectively. As such, HSD3B1 corresponds to the ZG-specific 3β-HSD isozyme in human adrenal gland [2]. Angiotensin II (AngII) and potassium (K^+) are the major physiological regulators of aldosterone synthesis. AngII stimulates expression of *HSD3B1* via the orphan nuclear receptors NGFIB and NURR1 in human adrenocortical H295R cells [3]. However, it remains unknown whether K^+ stimulation similarly activates this NGFIB/NURR1 pathway. Here I examined K^+ sensitivity of *HSD3B1* in H295R cells **(chapter 1)**. Furthermore, I extended my research to understanding the roles of this enzyme in other tissues. I found that Hsd3b6 is expressed in the meibomian glands of mouse eyelid. I explored the physiological function and regulatory mechanisms of this enzyme in the meibomian glands **(chapter 2)**.

Chapter 1: Stimulus-selective induction of the orphan nuclear receptor NGFIB underlies different influences of angiotensin II and potassium on the human adrenal gland zona glomerulosa-specific 3β-HSD isoform gene expression in adrenocortical H295R cells

I show that K^+ stimulation lacks the ability to induce *HSD3B1* expression in human adrenocortical H295R cells. Both AngII and K^+ were able to enhance transcription of the aldosterone synthase gene (*CYP11B2*). Promoter analysis revealed that although both AngII and K^+ activate transcription from the Ca^{2+}/cAMP response element (CRE) located in the *CYP11B2* promoter, the orphan nuclear receptor NGFIB-responsive element (NBRE) located in the *HSD3B1* promoter fails to respond to K^+, being only able to enhance transcription after AngII treatment. I found that induction of *de novo* protein synthesis of NGFIB occurs only after AngII treatment. This sharply contrasts with the phosphorylation that occurs in response to both AngII and K^+ on the CREB/ATF family transcription factor ATF2. Chromatin immunoprecipitation assay confirmed that the NGFIB protein occupies the *HSD3B1* promoter only after AngII, while ATF2 binds to the *CYP11B2* promoter in response to both AngII and K^+. These data provide evidence that signals from AngII and K^+ can be uncoupled in the regulation of *HSD3B1* in the human adrenocortical H295R cells [4].

Chapter 2: Age-associated pathogenesis of dry eye disease involves an attenuation of circadian clock-regulated 3β-HSD activity in the meibomian glands

Although it is well known that malfunction of the circadian clock is linked to the pathogenesis of a wide variety of diseases, it is unclear whether it affects the development of dry eye disease. Meibomian glands are holocrine glands embedded in the eyelid and secrete lipid onto the ocular surface tear film. Meibomian gland dysfunction (MGD) is the major cause of evaporative dry eye disease, especially in elderly patients. However, the molecular mechanisms by which aging contributes to MGD are poorly understood. I found that Hsd3b6 is specifically expressed in acinar epithelial cells of mouse meibomian gland. Notably, meibomian 3β-HSD enzymatic activity oscillates in a circadian fashion and declines with age. The meibomian glands from *Hsd3b6*-deficient mice did not show any noticeable 3β-HSD activity, demonstrating that Hsd3b6 is essential for the local steroid production within the meibomian glands. Finally, I provide evidence that the loss of meibomian 3β-HSD activity causes severe atrophy of meibomian glands and leads to dry eye disease. These findings suggest that age-associated attenuation of meibomian Hsd3b6 activity may underlie the development of MGD leading to dry eye disease.

References

[1] Doi *et al*., *Nat Med* **16**, 67–74, 2010

[2] Doi *et al*., *J Clin Endocrinol Metab* **99**, E257–62, 2014

[3] Ota *et al*., *Mol Cell Biol* **34**, 3880–94, 2014

[4] Yarimizu *et al*., *Endocrine J* **62**, 765–776, 2015

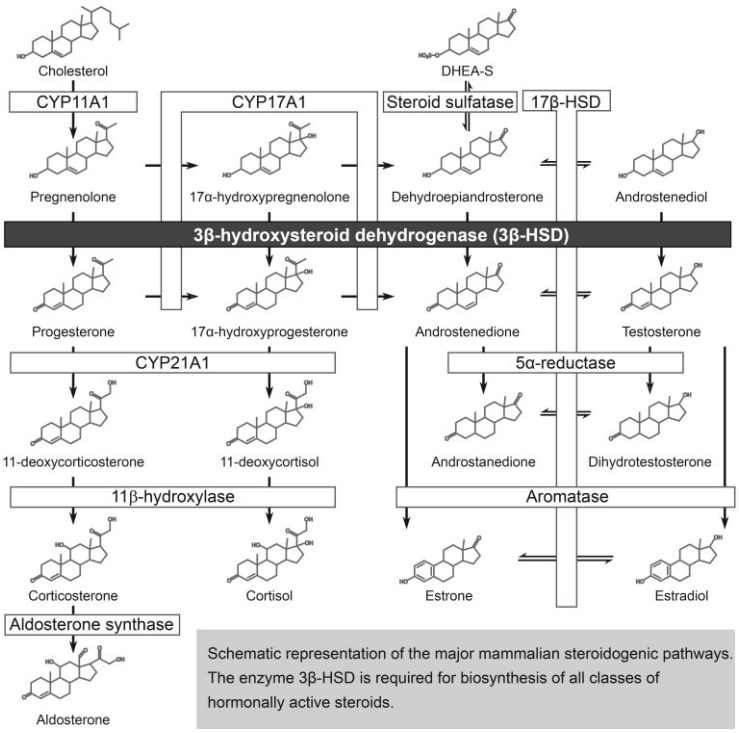

Schematic representation of the major mammalian steroidogenic pathways. The enzyme 3β-HSD is required for biosynthesis of all classes of hormonally active steroids.

Chapter 1

Stimulus-selective induction of the orphan nuclear receptor NGFIB underlies different influences of angiotensin II and potassium on the human adrenal gland zona glomerulosa-specific 3β-HSD isoform gene expression in adrenocortical H295R cells

Introduction

AngII and K^+ are the major physiological regulators of aldosterone synthesis. However, their respective roles in regulation of aldosterone synthesis are not well defined, particularly in terms of transcriptional regulation of steroidogenic enzyme genes. Aldosterone synthesis occurs exclusively in the adrenal zona glomerulosa (ZG) cells via a series of enzymatic reactions involving a number of enzymes. The 3β-hydroxysteroid dehydrogenase/Δ^5-Δ^4-isomerase (3β-HSD) is an enzyme that catalyzes the conversion of Δ^5-3-hydroxysteroids (e.g. pregnenolone) into hormonally active Δ^4-3-ketosteroids (e.g. progesterone) [1, 2], a step required for aldosterone synthesis. Whereas two distinct 3β-HSD isoforms (type I 3β-HSD encoded by *HSD3B1* and type II 3-βHSD encoded by *HSD3B2*) exist in humans, the type II 3β-HSD has long been considered the major or sole isoform present in the adrenal gland. However, the recent finding that type I 3β-HSD is expressed in ZG cells [3, 4] has revised the canonical view and raised a question as to whether the expression of this gene (*HSD3B1*) is under the control of AngII and K^+. By using human adrenocortical H295R cells as a model system, I recently showed that AngII could stimulate expression of *HSD3B1* [5]. I also showed that AngII-induced induction of *HSD3B1* requires *de novo* protein synthesis of the orphan nuclear receptors nerve growth factor IB (NGFIB) and nuclear receptor related 1 (NURR1). The *HSD3B1* promoter contains a functional

NGFIB/ NURR1-responsive element (NBRE) to which these proteins bind in response to AngII [5]. However, it remains unknown whether K^+ stimulation similarly activates this NGFIB/NURR1 pathway.

The aldosterone synthase, which is encoded by *CYP11B2*, catalyzes the final step of aldosterone synthesis [6]. Like *HSD3B1*, expression of *CYP11B2* is confined to ZG cells. It has been well established that AngII and K^+ can both activate transcription of *CYP11B2* through a common *cis*-regulatory element [7]. The *CYP11B2* promoter contains a Ca^{2+}/cAMP response element (CRE) to which the CREB/ATF family proteins bind in response to AngII and K^+ [8]. Thus, AngII and K^+ are thought to share, at least in part, the CREB/ATF-mediated transcription pathway. However, the extent of difference (or similarity) between AngII and K^+ in the regulation of other steroidogenic enzyme genes has remained unexplored.

Here I examined K^+ sensitivity of *HSD3B1* in H295R cells. Contrary to my naive expectation, I observed that K^+ stimulation was unable to enhance expression of *HSD3B1*. To understand the underlying mechanism better, I compared transcriptional regulation of *HSD3B1* with that of *CYP11B2*. The results presented in this study provide several lines of evidence that the NGFIB/NURR1-*HSD3B1* pathway operates only for AngII. This selectivity of action of NGFIB/NURR1 differs from the CREB/ATF-mediated transcription pathway that operates in response to both AngII and K^+.

Materials and Methods

Cell culture and treatments

Human adrenocortical H295R cells (ATCC CRL-2128) were cultured in Dulbecco's modified Eagle's medium/ Ham's F-12 (DMEM/F-12; Nacalai Tesque, Japan) supplemented with 2.5% Nu serum (BD Biosciences) and 1% ITS + Premix (BD Biosciences) in a 37°C humidified atmosphere (5% CO_2). Unless otherwise noted, cells were cultured in the above-mentioned serum-containing medium. For gene expression analysis, cells were seeded on 24-well plate at a density of 2×10^5 cells/well and cultured for 3 days before agonist stimulation. For stimulation, an aliquot of freshly reconstituted AngII (Peptide Institute, Japan) or KCl (for K^+ stimulation) was added to the culture medium at the indicated concentrations. Where specified, cycloheximide (CHX; final concentration, 10 μg/mL) was added to the medium 15 min before AngII or K^+ treatment. For the analysis of serum-starved cells, cells were cultured as described above except that the medium was replaced with DMEM/F-12 serum-free medium for the last 24 h.

RNA extraction and qRT-PCR analysis

Total RNA was extracted from cells using Sepasol-RNAI Super G (Nacalai Tesque). cDNA was synthesized by reverse transcription using random

hexamer primers and SuperScript III first-strand synthesis Super-Mix (Thermo). Quantitative PCR (qPCR) was run in duplicate with the primers and probes shown below. Because of the high sequence similarity between the human 3β-HSD isoform genes (*HSD3B1* and *HSD3B2*, 93.6% identity, including the 5' and 3' untranslated regions [UTRs]), qPCR analysis of the two genes was performed with a TaqMan PCR reagent (Thermo) using gene-specific TaqMan MGB probes. As our laboratory previously reported [4], these probes distinguish a few nucleotide differences at the region corresponding to the dehydrogenase catalytic Y-X-X-X-K motif [2] of the human 3β-HSDs. On the other hand, SYBR green-based qPCR was done for the other genes with the aid of a THUNDERBIRD SYBR qPCR Mix (TOYOBO, Japan). As a qPCR device, I used a Step-OnePlus real-time PCR monitoring system (Thermo), and the quantification of target cDNAs was achieved with a standard curve method as described previously [5]. The standard curve was generated by amplifying a dilution series of a standard DNA (ranging from 1 to 10,000 zmol), for which I used linearized plasmid DNA carrying the target amplicon. The data were normalized to the expression levels of the gene encoding ribosomal protein LP0 (*RPLP0*). The sequences for the primers and probes are as follows: for *CYP11B2*, forward primer 5'-ACT CGC TGG GTC GCA ATG-3' and reverse primer 5'-GTC TCC ACC AGG AAG TGC-3'; for *NGFIB*, forward primer 5'-GCC TTC CTG GAG CTC TTC ATC-3' and reverse primer 5'-GAG

AAG GCC AGG ATA CTG TCA ATC-3’; for *NURR1*, forward primer 5’-GGC TCC CAG AGG GAA CTG-3’ and reverse primer 5’-GAG TCC AGC CTG TCC AAT CTC-3’; for *NOR1*, forward primer 5’-TCC GCT CCT CCT ACA CTC TC-3’ and reverse primer 5’-GGT GTA TTC CGA GCT GTA TGT CTG-3’; for *CREB*, forward primer 5’-GTC TCC ACA AGT CCA AAC AGT-3’ and reverse primer 5’-ATG GCA GGT GCT GAA GTC-3’; for *ATF1*, forward primer 5’-CAT CCG ACA GCA TAG GCT CC-3’ and reverse primer 5’-CTC CAT CTG TGC CTG GAC TT-3’; for *ATF2*, forward primer 5’-GAG TTG GCG AGT CCA TTT GAG-3’ and reverse primer 5’-GAT GTG GGC TGT GCA GTT TGT G-3’; for *RPLP0*, forward primer 5’-ATG CAG CAG ATC CGC ATG T-3’ and reverse primer 5’-TTG CGC ATC ATG GTG TTC TT-3’; for *HSD3B1*, forward primer 5’-AGA AGA GCC TCT GGA AAA CAC ATG-3’, reverse primer 5’-TAA GGC ACA AGT GTA CAG GGT GC-3’, and probe 5’-FAM-CCA TAC CCA CAC AGC-MGB-3’ (where FAM is 6-carboxyfluorescein); and for *HSD3B2*, forward primer 5’-AGA AGA GCC TCT GGA AAA CAC ATG-3’, reverse primer 5’-CGC ACA AGT GTA CAA GGT ATC ACC A-3’, and probe 5’-VIC-TCC ATA CCC GTA CAG CA-MGB-3’ (where VIC is 2’-chloro-7’-phenyl-1,4-dichloro-6-carboxyfluorescein).

Plasmids, transfection, and real-time luciferase monitoring

The following reporter plasmids were used in this study: (i) *HSD3B1* NBRE-luc, in which a DNA fragment containing nine tandem copies of the sequence corresponding to the *HSD3B1* NBRE with its flanking sequences (positions −130 to −110) was inserted into the pGL4.23 (luc2/minP) vector (Promega); and (ii) *CYP11B2* CRE-luc, in which a DNA fragment containing nine tandem copies of the sequence corresponding to the *CYP11B2* CRE with its flanking sequences (positions −82 to −61) was inserted into the pGL4.23 vector. Cells were transfected with 500 ng reporter plasmids using the Lipofectamine LTX/Plus reagent (Thermo) according to the manufacturer's instructions. Six hours after transfection, the medium was replaced with the fresh one. After overnight recovery, the medium was changed to 1 mM D-luciferin-containing medium, and cells were transferred to a dish-type photon countable luminometer (Kronos Dio, ATTO) under 5% CO_2 atmosphere at 37°C. The luminescence was monitored for 2 min at 20 min intervals. Two days later, cells were treated with either AngII or K^+ at the indicated concentration. All values were normalized to the means of bioluminescence during 4 hours before stimulation.

Western blotting

Cells were harvested in Laemmli buffer, and immunoblotting was performed as described [5] with the following antibodies toward NGFIB (1:500 dilution; M-210 antibody; Santa Cruz Biotechnology), NURR1 (1:1,000 dilution; N1404 antibody; Perseus Proteomics), NOR1 (1:500 dilution; H7833 antibody; Perseus Proteomics), phospho-ATF2 (1:500 dilution; 9221 antibody; Cell Signaling Technology), and ATF2 (1:1,000 dilution; C-19 antibody; Santa Cruz Biotechnology). Densitometric quantification of phospho-ATF2 bands was performed by using Multi Gauge software (Fuji Film, Japan).

Chromatin immunoprecipitation (ChIP)

ChIP assay was performed as described [5] with modifications. H295R cells grown to confluence on 10 cm dish (~1×10^7 cells) were treated with AngII (100 nM), K^+ (16 mM), or vehicle (PBS) for 4 h. For NGFIB-ChIP, cells were removed from culture dish and immediately homogenized in phosphate-buffered saline (PBS) containing 2 mM disuccinimidyl glutarate (Thermo), and the homogenates were kept at room temperature for 20 min. Formaldehyde was then added at 1% of final concentration and incubated for a further 5 min. Cross-linking reactions were stopped by glycine (final concentration, 150 mM) on ice. The homogenates were centrifuged at 700

× *g* for 10 min, and the resultant nuclear pellets were washed twice with ice-cold PBS. The nuclei were resuspended in immunoprecipitation (IP) buffer (10 mM Tris-HCl, pH 8.0, 150 mM NaCl, 1 mM EDTA, 1% Triton X-100, 0.1% sodium deoxy- cholate, 1 mM phenylmethylsulfonyl fluoride [PMSF], protease inhibitor cocktail [Roche]) and sonicated 10 times for 30 sec each time at 4°C using a Bioruptor UCW-201TM apparatus (Tosho Denki, Japan). Approximately 1.8 μg fragmented chromatin was immunoprecipitated with 1 μg of anti-NGFIB/NURR1 antibody, which recognizes both NGFIB and NURR1 (E-20 antibody; Santa Cruz Biotechnology) For ATF2-ChIP, cells were homogenized in PBS containing 1% formaldehyde and kept at room temperature for 10 min. Following addition of glycine and wash, the nuclei were resuspended in lysis buffer (50 mM Tris-HCl, pH 8.0, 10 mM EDTA, 1% sodium dodecyl sulfate, 1 mM PMSF, PhosSTOP phosphatase inhibitors [Roche], protease inhibitor cocktail) and sonicated 5 times for 30 sec each time at 4°C using a Bioruptor apparatus. The lysates were diluted ten times with IP buffer, and 6 μg fragmented chromatin was immunoprecipitated with 1 μg of anti-ATF2 antibody (C-19 antibody; Santa Cruz Biotechnology). Immunoprecipitated DNA fragments were quantified by either TaqMan qPCR (for *HSD3B1* and *HSD3B2*) or SYBR green-based qPCR (for *CYP11B2*) with the following primers and probe: for *HSD3B1* promoter, forward primer 5'-CCT GTT AAG GCT AAA CCC AAG AC-3', reverse

primer 5'-CAT TGC TCT CTC CTC CTA TGG G-3', and TaqMan probe 5'-VIC-TGC CAC ACT GCA GCA TTA GGA TGG G-TAMRA-3'; for *HSD3B2* promoter, forward primer 5'-ACT GAC CAG TGT TCT GTT AAG GCT AAA G-3', reverse primer 5'-CAT TGC TCC CTC CTC CTC CAG A-3', and TaqMan probe 5'-VIC-CTT TAT CAC ACT GTG GCC TTA AGA TTG GAT TTC TC-TAMRA-3'; for *CYP11B2* promoter, forward primer 5'-CCC ACG CCT TTT CTC AGC ATC-3' and reverse primer 5'-AAT GCT CCC TCC ACC CTG TTC-3'.

Statistical analysis

I used two-way analysis of variance (ANOVA) with Bonferroni *post hoc* test to evaluate mean differences between different groups with different treatments in ChIP assay. A value of $P < 0.01$ was taken as significant.

Results

K^+ does not enhance *HSD3B1* expression.

The adrenocortical H295R cells were treated with K^+ over a range of periods (1, 2, 4, 8, and 12 h) at a concentration of 8 mM (**Fig. 1A**) or 16 mM (**Fig. 1B**), and total RNA was extracted from the cells and analyzed by qRT-PCR using gene-specific TaqMan MGB probes and primers for *HSD3B1* and *HSD3B2*. Due to a high degree of cDNA sequence similarity between *HSD3B1* and *HSD3B2* (93.6% identity, including the 5'- and 3'-untranslated regions), mRNA expression profiles of *HSD3B1* and *HSD3B2* have never been strictly characterized in K^+-treated adrenal cells [9-11]. In agreement with previous studies, K^+ treatment increased expression of the aldosterone synthase gene *CYP11B2* [12] (**Fig. 1**). The levels of *CYP11B2* mRNA in H295R cells were dose-dependently increased to about 6-fold or 25-fold over basal levels after 8 mM or 16 mM K^+ treatment, respectively. However, expression levels of *HSD3B1* and *HSD3B2* were almost constant throughout the K^+ treatment even under 16 mM condition (**Fig. 1A, B**). These results demonstrate that K^+-induced intracellular signaling that leads to *CYP11B2* expression cannot enhance expression of 3β-HSD genes. Importantly, this was also the case when the cells were serum-starved prior to K^+ stimulation (**Fig. 1C, D**).

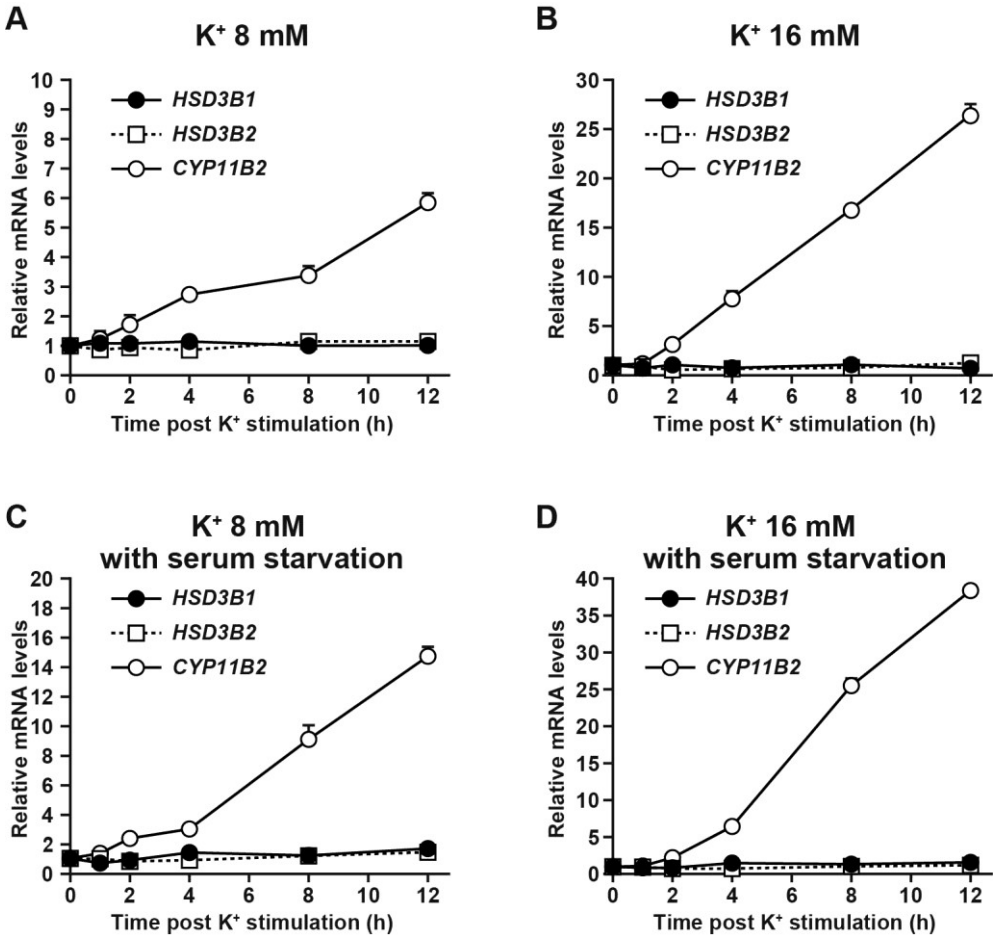

Figure 1 The effect of K^+ on the expression of *HSD3B1*, *HSD3B2*, and *CYP11B2*. (A−D) Gene expression profiles of *HSD3B1* (filled circle), *HSD3B2* (square), and *CYP11B2* (open circle) after K^+ treatment in H295R cells. KCl was added to the culture medium at a final concentration of 8 mM (A, C) or 16 mM (B, D). After the indicated periods of time, total RNA was isolated from the cells and the levels of *HSD3B1*, *HSD3B2*, and *CYP11B2* mRNA were determined by qRT-PCR. For (A) and (B), cells were cultured in a standard medium containing 2.5% Nu serum. For (C) and (D), cells were serum-starved prior to stimulation. Values (means ± SEM, n = 3) are normalized to the levels of *RPLP0* and plotted relative to those at time 0.

K^+ treatment was next performed in conjunction with AngII (**Fig. 2**). As reported, AngII treatment increased expression of *HSD3B1* [5] (**Fig. 2A**). Importantly, however, expression levels of *HSD3B1* were not further increased by a simultaneous treatment with AngII and K^+ (**Fig. 2A**). Thus K^+ treatment does not enhance *HSD3B1* expression even in the presence of AngII. As shown in **Fig. 2B**, AngII was unable to induce *HSD3B2* [5]. Again, K^+ stimulation had no effect on *HSD3B2* expression, regardless of whether administered alone or in combination with AngII (**Fig. 2B**). Forskolin treatment, on the other hand, could increase expression of *HSD3B2* (**Fig. 2B**) as previously suggested [9, 13-16]. Thus, the responsiveness of this gene relies on the type of agonists administered to the cells.

To assess relative expression levels between *HSD3B1* and *HSD3B2* in H295R cells, I determined absolute mRNA levels for each gene (**Fig. 2C**). At the basal levels, *HSD3B2* was approximately 8 times higher than *HSD3B1* (40.7 ± 1.2 mmol/mol for *HSD3B1* v.s. 347.8 ± 65.1 mmol/mol for *HSD3B2*; the values (means ± SEM, n=3) were normalized with *RPLP0*). On the other hand, after AngII stimulation, *HSD3B1* mRNA was dramatically increased to the levels almost equal to or higher than those of *HSD3B2* (323.2 ± 18.8 mmol/mol for *HSD3B1* v.s. 249.2 ± 20.8 mmol/mol for *HSD3B2*). Thus, in addition to the responsiveness to AngII, *HSD3B1* and *HSD3B2* are different in the steady-state basal levels in H295R cells.

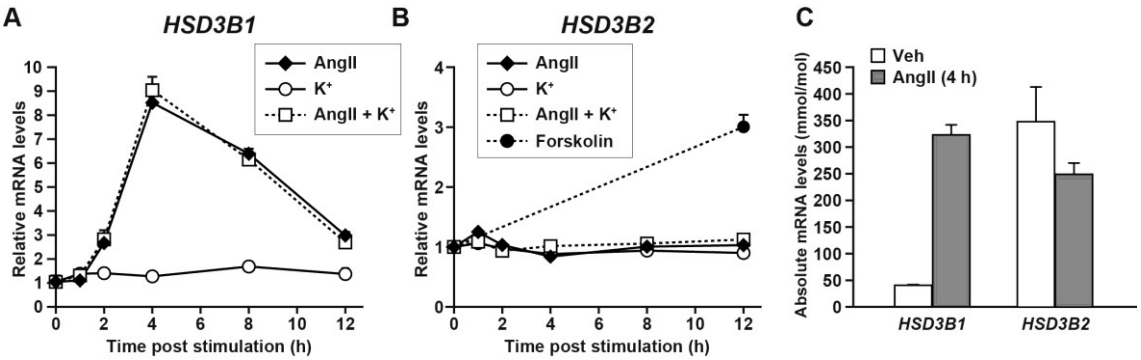

Figure 2 K^+ does not increase expression of *HSD3B1* or *HSD3B2* even in the presence of AngII. (A) Expression profiles of *HSD3B1* in H295R cells after treatment with K^+ (16 mM) alone or in combination with AngII (100 nM). Values (means ± SEM, n = 3) were determined as described in **Fig. 1**. (B) Expression profiles of *HSD3B2* in H295R cells after treatment with K^+ (16 mM) alone or in combination with AngII (100 nM). For control, cells were treated with forskolin (10 μM) for 12 h. Values are means ± SEM (n = 3). (C) Absolute mRNA levels of *HSD3B1* and *HSD3B2* in H295R cells after treatment with AngII (100 nM) or vehicle (Veh) for 4 h. qRT-PCR was performed with a standard curve method, and the values were normalized with the expression levels of *RPLP0* (means ± SEM, n = 3).

Different effects of K^+ and AngII on expression of *HSD3B1* and *CYP11B2*

H295R cells were treated with AngII (100 nM) or K^+ (16 mM) in the presence or absence of the protein synthesis inhibitor cycloheximide (CHX) (**Fig. 3**). Both AngII and K^+ evoked induction of *CYP11B2* in a CHX-independent manner. In contrast, *HSD3B1* increased only after AngII treatment, and this induction was completely blocked by CHX. These profiles, observed here, are basically the same as what I reported previously [5] and confirmed that the increment of *HSD3B1* expression relies on *de novo* protein synthesis. The induction kinetics also differs between *HSD3B1* and *CYP11B2*. *HSD3B1* began to increase 2 h after AngII treatment, and it increased rapidly to about 6-fold over basal level by 4 h. Following the peak at 4 h, the levels of *HSD3B1* mRNA decreased gradually. In contrast, the levels of *CYP11B2* mRNA continued to increase over the course of 12 h treatment with AngII and K^+. These data suggest that the underlying mechanisms that control expression of *HSD3B1* and *CYP11B2* are different.

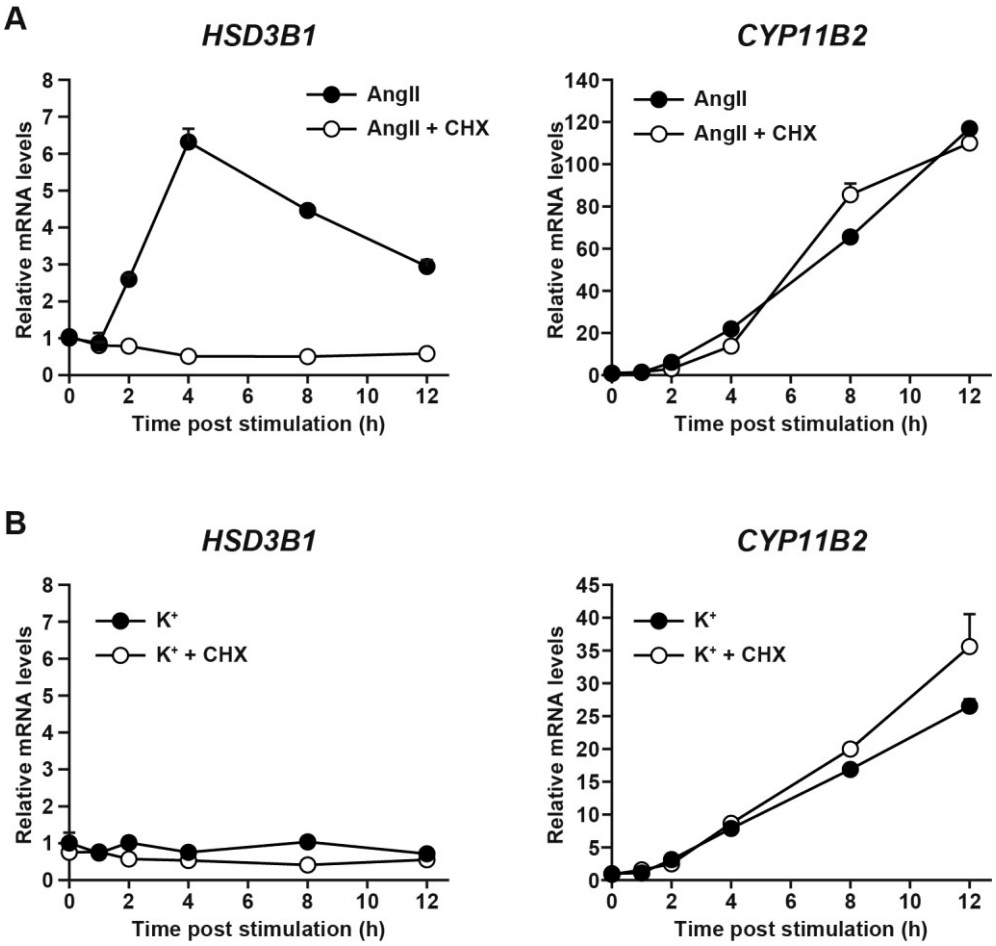

Figure 3 *HSD3B1* does not increase in response to K^+, despite displaying an overt increase in response to AngII, a situation different from *CYP11B2*. (A)(B) Responsiveness of *HSD3B1* and *CYP11B2* to treatment with AngII (100 nM, A) or K^+ (16 mM, B) in the presence (open circle) or absence (filled circle) of cycloheximide (CHX, 10 µg/ml) in H295R cells. After the indicated periods of time, total RNA was isolated from the cells and the levels of *HSD3B1*, *HSD3B2*, and *CYP11B2* mRNA were determined by qRT-PCR. Values (means ± SEM, n = 3) are normalized to the levels of *RPLP0* and plotted relative to those at time 0 without CHX treatment.

Different effects of K^+ and AngII on *HSD3B1* promoter NBRE enhancer activity

Why does K^+-induced intracellular signaling lack the ability to induce *HSD3B1*? Our laboratory previously demonstrated that AngII leads to induction of *HSD3B1* through *de novo* protein synthesis of the orphan nuclear receptors NGFIB and NURR1 [5]. These proteins bind to the cognate NBRE sequence of the *HSD3B1* promoter and enhance transcription [5]. K^+ signaling, therefore, might not be able to enhance transcription through the NBRE site. To test this hypothesis, a luciferase reporter vector containing multiple copies of the NBRE sequence of *HSD3B1* (*HSD3B1* NBRE-luc) was transfected into H295R cells, and bioluminescence was monitored in culture over a course of treatment with AngII or K^+ (**Fig. 4A**). Interestingly, robust induction of reporter activity was observed only after AngII treatment (**Fig. 4A**). K^+ treatment failed to induce reporter gene expression through the NBRE site (**Fig. 4A, C, D**).

Equivalent effects of K^+ and AngII on *CYP11B2* promoter CRE enhancer activity

The *CYP11B2* promoter contains a consensus CRE [7, 17]. To compare the responsiveness of the CRE with that of the NBRE, a luciferase vector containing multiple copies of the isolated CRE sequence of *CYP11B2*

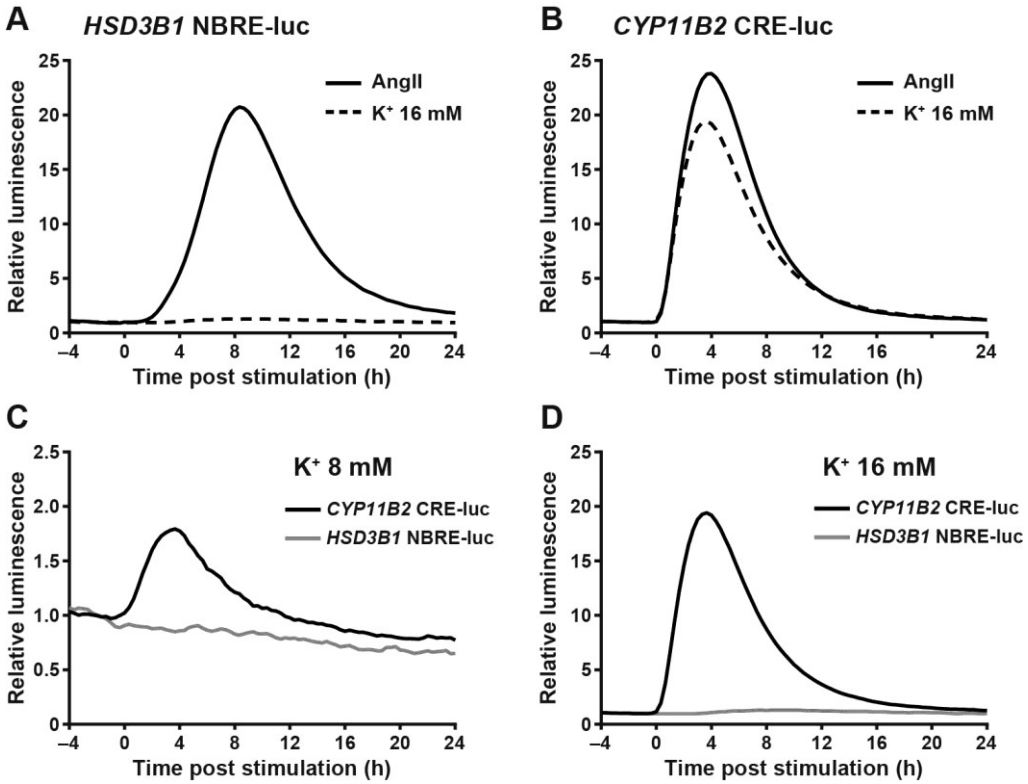

Figure 4 Transcriptional enhancer activity of the NBRE site of *HSD3B1* does not increase in response to K^+, despite displaying an overt increase in response to AngII, a profile different from that of the CRE site of *CYP11B2*. (A)(B) Luciferase reporter gene expression from the NBRE site of *HSD3B1* (A) and the CRE site of *CYP11B2* (B) after stimulation with 100 nM AngII (black line) or 16 mM K^+ (dashed line) in H295R cells. (C)(D) Luciferase reporter gene expression from the CRE site of *CYP11B2* (black) and the NBRE site of *HSD3B1* (gray) after stimulation with 8 mM K^+ (C) or 16 mM K^+ (D) in H295R cells. Cells were transfected with a reporter vector containing either multiple copies of the NBRE site of *HSD3B1* (*HSD3B1* NBRE-luc) or the CRE site of *CYP11B2* (*CYP11B2* CRE-luc). Traces show representative bioluminescence monitored before and after each treatment. Similar traces were obtained in three independent experiments.

(*CYP11B2* CRE-luc) was transfected into H295R cells and monitored for the response to AngII and K^+ (**Fig. 4B−D**). In agreement with the endogenous *CYP11B2* mRNA expression profiles (**Figs. 1** and **3**), both AngII and K^+ caused a significant enhancement of the CRE-luc reporter activity with an amplitude of ~25-fold for AngII (**Fig. 4B**), ~2-fold for 8 mM K^+ (**Fig. 4C**), and ~20-fold for 16 mM K^+ (**Fig. 4B, D**). These results indicate that the CRE is a common element for AngII and K^+ activity [6, 7].

The orphan nuclear receptor NGFIB family members do not increase in response to K^+.

The orphan nuclear receptor NGFIB family contains three members, NGFIB, NURR1, and NOR1. It has been well established that AngII can stimulate mRNA expression of *NGFIB*, *NURR1*, and *NOR1* [5, 18, 19]. However, K^+ responsiveness of this gene family remains unclear [20, 21]. Moreover, to date, there have been no studies that assess the protein levels of NGFIB, NURR1, and NOR1 in K^+-stimulated H295R cells. Therefore, to gain a better picture of this family, I assessed absolute mRNA levels (**Fig. 5A, B**) and protein expression profiles (**Fig. 5C**) of all the NGFIB members in H295R cells after treatment with either AngII or K^+. The mRNA levels of *NGFIB*, *NURR1*, and *NOR1* were all rapidly increased

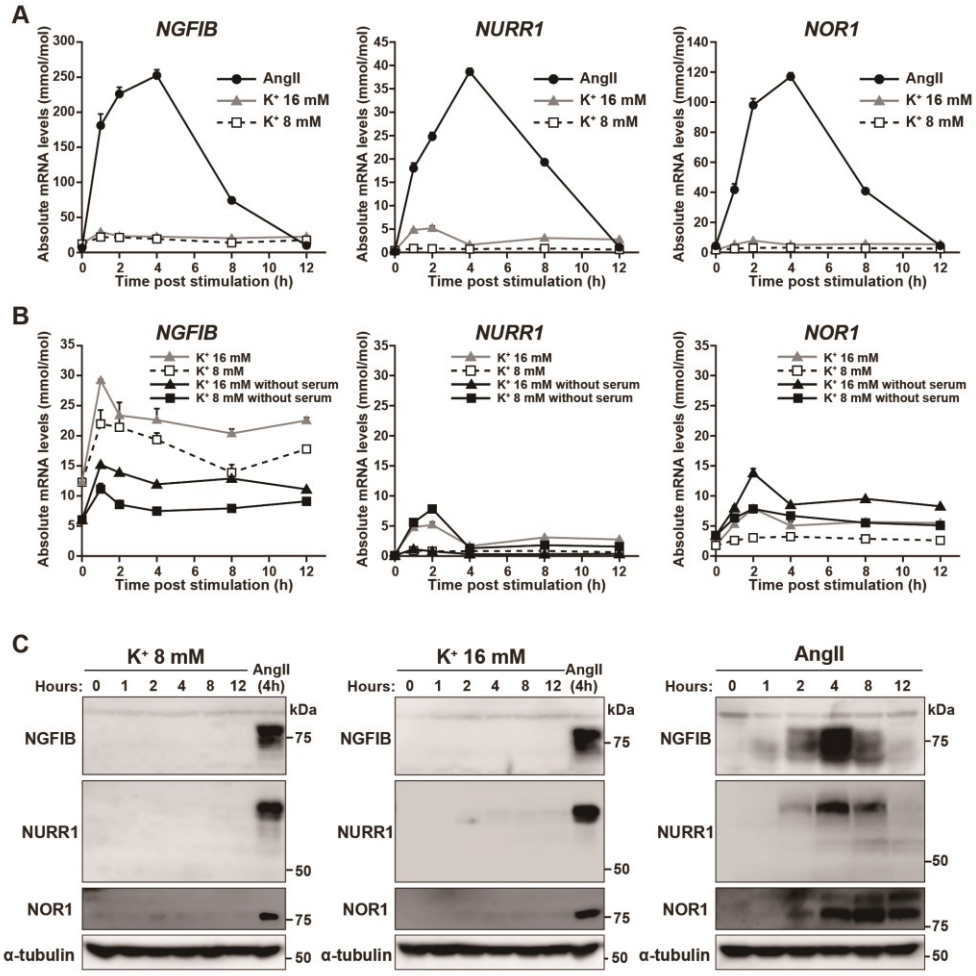

Figure 5 The orphan nuclear receptor NGFIB family members do not increase in response to K^+, despite displaying an overt increase in response to AngII. (A) Gene expression profiles of *NGFIB* (left), *NURR1* (middle), and *NOR1* (right) after stimulation with 100 nM AngII (circle), 16 mM K^+ (triangle), or 8 mM K^+ (square) in H295R cells. Culture medium contains 2.5 % Nu serum. After the indicated periods, total RNA was isolated from the cells, and absolute mRNA levels of *NGFIB*, *NURR1*, and *NOR1* were determined by qRT-PCR. Values (means ± SEM, n = 3) are normalized to the levels of *RPLP0*. (B) Absolute mRNA levels of *NGFIB* (left), *NURR1* (middle), and *NOR1* (right) in serum-starved H295R cells after stimulation with 8 mM K^+ or 16 mM K^+. For comparison, the data shown in (A) were replotted in parallel. (C) Western blots showing the protein expression profiles of NGFIB (upper), NURR1 (middle), and NOR1 (lower) after AngII (100 nM) or K^+ (8 mM or 16 mM) stimulation in H295R cells. The culture medium used here contains 2.5 % Nu serum.

after AngII treatment by approximately 40-, 200-, and 25-fold over basal levels, respectively, and their peak values were: 252.4 ± 8.1 mmol/mol for *NGFIB*, 38.7 ± 0.7 mmol/mol for *NURR1*, and 117.0 ± 2.5 mmol/mol for *NOR1* (**Fig. 5A**). On the other hand, however, K^+ treatment produced only a faint peak mRNA expression for *NGFIB* (22.0 ± 2.3 mmol/mol for 8 mM K^+; 29.2 ± 0.2 mmol/mol for 16 mM K^+), *NURR1* (0.9 ± 0.1 mmol/mol for 8 mM; 5.2 ± 0.4 mmol/mol for 16 mM), and *NOR1* (3.2 ± 0.2 mmol/mol for 8 mM; 7.9 ± 0.2 mmol/mol for 16 mM) (**Fig. 5A**). As shown in **Fig. 5B**, serum-starved H295R cells also show similar peak expression values for *NGFIB* (11.1 ± 0.9 mmol/mol for 8 mM K^+; 15.2 ± 0.4 mmol/mol for 16 mM K^+), *NURR1* (1.2 ± 0.1 mmol/mol for 8 mM; 7.8 ± 0.2 mmol/mol for 16 mM), and *NOR1* (7.8 ± 0.5 mmol/mol for 8 mM; 13.8 ± 0.4 mmol/mol for 16 mM). I therefore conclude that while K^+ appears to be able to enhance mRNA expression for each gene to some extent (**Fig. 5A, B**), the respective peak absolute mRNA levels are considerably low, compared to that seen for AngII treatment. Furthermore, to test the consequence of this modest mRNA expression, I performed Western blot analysis (**Fig. 5B**) and found that K^+ treatment failed to induce detectable protein expression of the NGFIB, NURR1, and NOR1 proteins. After AngII treatment, expression of these proteins was remarkably increased (**Fig. 5A**). Thus, substantial protein induction of the members of the NGFIB family occurs only after AngII treatment.

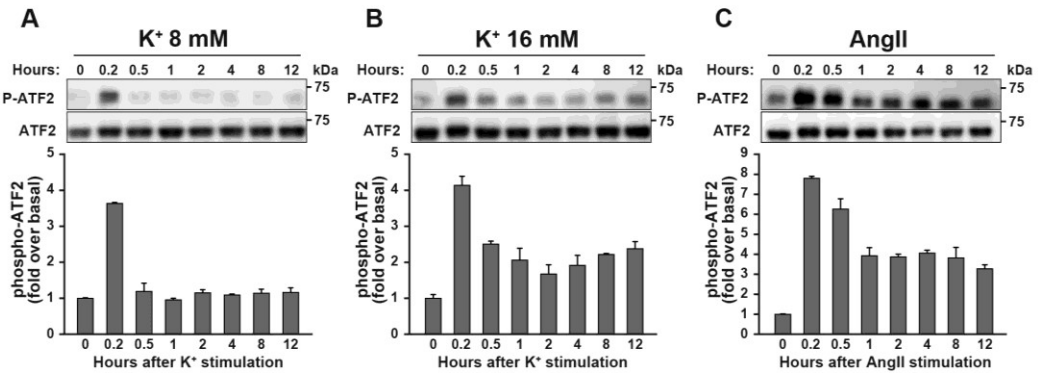

Figure 6 Both K^+ and AngII induce phosphorylation of ATF2 in H295R cells. (A)(B)(C) Western blots showing time-dependent phosphorylation profiles of ATF2 after stimulation with 8 mM K^+ (A), 16 mM K^+ (B), or 100 nM AngII (C) in H295R cells. Whole cell lysates were blotted and probed with the antibodies indicated. Relative band intensities of phospho-ATF2 were determined by densitometry. Data are the means ± variation from two independent experiments.

Both K^+ and AngII induce phosphorylation of the CREB/ATF family member ATF2.

In contrast to the stimulus-selective induction of the NGFIB family proteins, I found that phosphorylation of ATF2 occurs in response to both AngII and K^+ (**Fig. 6**). ATF2 was analyzed here because it has been reported [8] that in H295R cells mRNA levels of ATF2 are relatively high (7.8 nmol/mol) compared to those of the other members, such as CREB (3.2×10^{-3} nmol/mol) and ATF1 (3.2 nmol/mol) [values in parentheses indicate absolute mRNA concentrations relative to *RPLP0*; see **Materials and Methods**]. As shown in **Fig. 6**, Western blot analysis revealed that phosphorylated protein levels of ATF2 were increased to ~7.5-, ~3.5-, or ~4.0-fold above basal values within 0.2 h after treatment with AngII, 8 mM K^+ or 16 mM K^+, respectively. Total ATF2 contents remained invariable throughout the treatments. There have been no studies that determined K^+-induced phosphorylation profiles of the CREB/ATF family in H295R cells. My data therefore demonstrate for the first time that K^+ treatment can dose-dependently induce ATF2 phosphorylation in H295R cells.

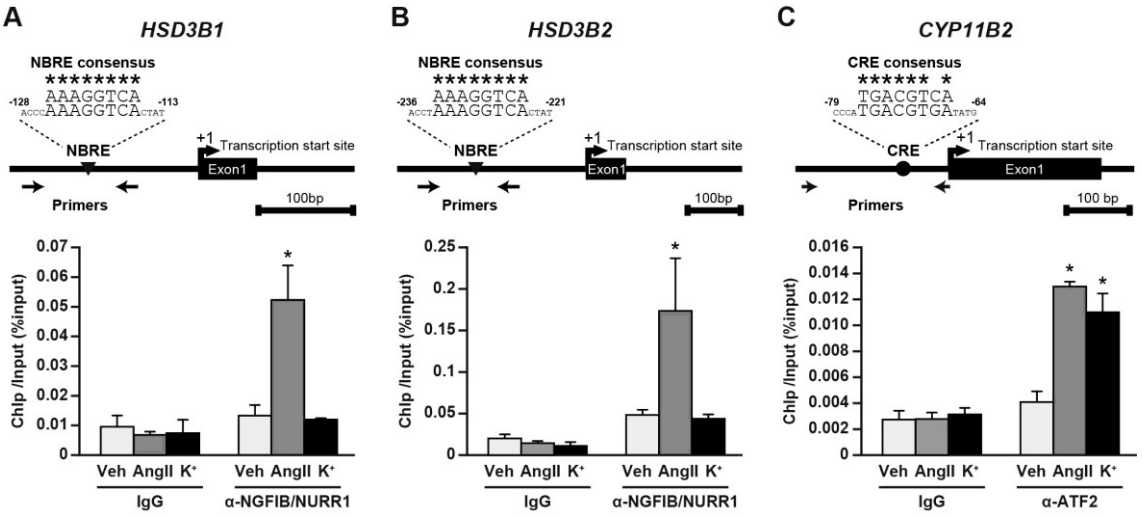

Figure 7 NGFIB binding to the *HSD3B1* NBRE site does not increase in response to K^+, despite displaying an increase in response to AngII, a situation different from ATF2 binding to the *CYP11B2* CRE site. (A−C) Upper: schematic genomic structure of *HSD3B1* (A), *HSD3B2* (B), and *CYP11B2* (C). Numbers, the positions relative to the transcription initiation site (position +1); *, sequences that conform to the consensus sequences of NBRE (A, B) and CRE (C); arrows, positions of primers used in ChIP assay. Lower: ChIP of *HSD3B1* (A), *HSD3B2* (B), and *CYP11B2* (C). After treatment with vehicle, AngII (100 nM), or K^+ (16 mM), cross-linked nuclear extract from H295R cells were subject to ChIP assay with anti-NGFIB/NURR1 (A, B) or anti-ATF2 (C). anti-NGFIB/NURR1 recognizes both NGFIB and NURR1. Normal rabbit IgG was used as a control for immunoprecipitation. ChIP values are expressed as a percentage of the input amount of chromatin. Values are means ± SEM of three independent samples. Veh, vehicle control treatment. *, $P < 0.01$ compared with vehicle control, Bonferroni test.

AngII, but not K^+, induces NGFIB recruitment to the *HSD3B1* promoter.

Finally, I performed chromatin immunoprecipitation (ChIP) assays to validate the impacts of AngII and K^+ on NGFIB/NURR1 protein recruitment to the promoter region of *HSD3B1*. Cells were incubated with AngII (100 nM), K^+ (16 mM), or control vehicle for 4 h. Then, cross-linked, sheared chromatin fragments were immunoprecipitated with either normal IgG or anti-NGFIB/NURR1 antibody. DNA fragments from the immunoprecipitates were examined by qPCR with a sequence-specific TaqMan probe and primers for the promoter region of *HSD3B1* (**Fig. 7A**). AngII significantly increased the levels of NGFIB/NURR1 binding to the promoter of *HSD3B1* (~3.9-fold over the vehicle control, $P < 0.01$). Importantly, however, K^+ treatment did not cause any observable effect on the ChIP values, relative to the vehicle control (**Fig. 7A**), revealing that significant recruitment of NGFIB/NURR1 occurs only after AngII treatment. AngII-specific recruitment of NGFIB/NURR1 was also observed for *HSD3B2* promoter (**Fig. 7B**) that bears a consensus NBRE sequence reported to be important for its response to ACTH [10]. In order to compare the responsiveness of NGFIB/NURR1 with that of ATF2, I then performed anti-ATF2 ChIP assay for the promoter of *CYP11B2* (**Fig. 7C**). As previously shown by Nogueira & Rainey [8], both AngII and K^+ significantly increased the levels of ATF2 recruitment to the promoter

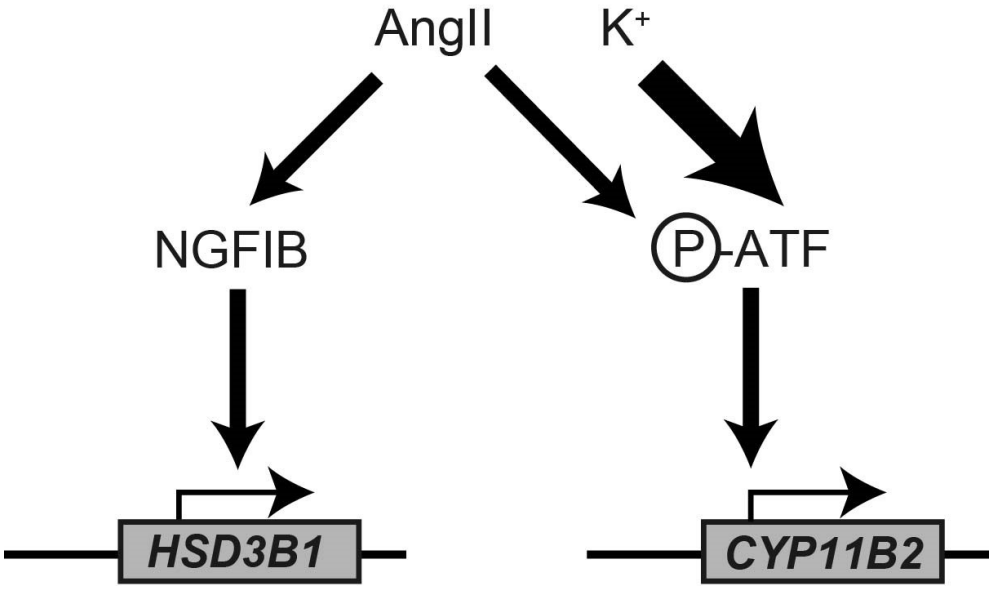

Figure 8 A model showing different responsiveness of *HSD3B1* and *CYP11B2* to AngII and K^+. *HSD3B1* responds to AngII, but not to K^+, due to AngII-selective induction of the NGFIB nuclear receptor family proteins. In contrast, *CYP11B2* responds to both stimuli through a common mechanism involving the activation (phosphorylation) of the CREB/ATF family members.

region of *CYP11B2* (~3.2- and ~2.7-fold over vehicle control, respectively), confirming that the *CYP11B2* CRE sequence serves as a common element for AngII and K^+ [6, 7].

Discussion

It has been well established that both AngII and K^+ activate transcription of *CYP11B2* in H295R cells. Based on this observation, AngII and K^+ are thought to share their downstream signals, at least in part, for the regulation of *CYP11B2*. In the present study, I revealed that signals from AngII and K^+ could be uncoupled in the regulation of *HSD3B1* in H295R cells. As depicted in **Fig. 8**, *HSD3B1* responds to AngII, but not K^+, due to AngII-selective induction of the NGFIB nuclear receptor family proteins. In contrast, *CYP11B2* responds to both stimuli through a common mechanism involving the activation (phosphorylation) of the CREB/ATF family members [8].

AngII and K^+ are the major physiological regulators of aldosterone synthesis. However, their respective roles in the regulation of steroidogenic genes are not fully understood. The CREB/ATF pathway is operative for both AngII and K^+ [6], and so this pathway cannot account for a possible difference between the two stimuli. Microarray studies suggest that down-stream signals from AngII and K^+ are not identical; a different set of genes was reported to be induced in response to AngII and K^+ in H295R cells [21], although the underlying mechanism(s) remains unknown. In the present study, I showed that the NGFIB/NURR1 pathway leading to *HSD3B1* expression is only operative for AngII. The current data therefore suggest that the pathways involving the orphan nuclear receptor NGFIB

family members would be one of the key elements that diversify the downstream signals from AngII and K^+.

There are a number of studies that describe AngII treatment-induced activation of *NGFIB*, *NURR1*, and *NOR1* in H295R cells [5, 18, 19]. However, K^+ responsiveness of this gene family has remained unclear [20, 21]. For example, microarray data presented by Romero *et al*. indicate that although K^+ stimulation tends to increase expression of *NGFIB*, *NURR1*, and *NOR1* in H295R cells, these increases did not reach significance [21]. To gain a complete picture, I therefore assessed mRNA and protein expression profiles of all the NGFIB family members in K^+-treated H295R cells. Interestingly, K^+ treatment could increase expression of this gene family, but the incremental increase of each member was modest, with the peak absolute mRNA levels of each gene remarkably less than those for AngII treatment. This modest mRNA induction was not accompanied by detectable protein expression. Moreover, in combination with the data from the ChIP and luciferase reporter-based promoter assays, I conclude that K^+ cannot evoke functional activation of the NGFIB family members.

HSD3B2 did not respond to AngII or K^+. Based on the measurement of absolute mRNA levels of *HSD3B1* and *HSD3B2*, I noticed that the steady-state basal levels of *HSD3B2* are relatively high, compared to those of *HSD3B1*. ChIP assay indicates that AngII could induce binding of NGFIB/NURR1 to the promoter of *HSD3B2*. Currently, I do not know why

this binding did not bring about any obvious induction of *HSD3B2* mRNA after treatment with AngII. Although the underlying mechanism needs to be clarified, one possible explanation might be that because of the relatively high steady-state mRNA expression levels of *HSD3B2*, the recruitment of NGFIB/NURR1 alone may not suffice to produce overt changes in the net amount of this transcript in H295R cells.

The current study also advanced my understanding of *CYP11B2*. It was previously demonstrated that the CRE enhancer element of the *CYP11B2* promoter is required for the normal transcriptional response of *CYP11B2* to AngII and K^+ [6, 7]. However, the previous studies were based on "single time point" luciferase assays, thus leaving a question as to "time course" of the response. In the present study, based on real-time bioluminescence measurement, I monitored the dynamics of *CYP11B2* CRE activity and found that its response is very rapid and transient, peaking at around 4 h after stimulation with AngII and K^+. This dynamics, interestingly, differs from that of the endogenous *CYP11B2* mRNA, which continued to increase with time during the course of a 12 h treatment with AngII and K^+. Therefore, it is interesting to speculate that the CRE might serves as a "trigger" for the subsequent continuous elevation of *CYP11B2*. There could be many plausible explanations for this model. For example, continuous chromatin remodeling and/or stabilization of transcripts of *CYP11B2* may be involved. CHX treatment also suggests that this process

should not depend on *de novo* protein synthesis. Future studies will be required to understand the mechanism of continuous upregulation of *CYP11B2*.

In summary, I showed that AngII and K^+ could evoke distinct intracellular signaling in H295R cells. Treatment of the cells with AngII, but not with K^+, resulted in activation of NGFIB family members and in turn enhanced expression of *HSD3B1*, whereas both treatments evoked expression of *CYP11B2* through activation of the CREB/ATF family member(s). The human H295R adrenocortical cell is one of the most characterized cellular models for the analysis of adrenal cell biology [22]. The relevance of my finding in physiology and diseases such as for better understanding of gene regulatory mechanism in aldosterone-producing adenoma (APA) and idiopathic hyperaldosteronism (IHA) will need further exploration. Aldosterone synthesis is a complex process potentially subject to many levels of regulation by AngII and K^+. Thus, a comprehension of differential regulation of *HSD3B1* and *CYP11B2* would help to understand the multi-modal regulation of steroidogenesis by AngII and K^+.

References

1. Payne, A.H., and Hales, D.B. (2004). Overview of steroidogenic enzymes in the pathway from cholesterol to active steroid hormones. Endocr Rev *25*, 947-970.
2. Simard, J., Ricketts, M.L., Gingras, S., Soucy, P., Feltus, F.A., and Melner, M.H. (2005). Molecular biology of the 3beta-hydroxysteroid dehydrogenase/delta5-delta4 isomerase gene family. Endocr Rev *26*, 525-582.
3. Doi, M., Satoh, F., Maekawa, T., Nakamura, Y., Fustin, J.M., Tainaka, M., Hotta, Y., Takahashi, Y., Morimoto, R., Takase, K., et al. (2014). Isoform-specific monoclonal antibodies against 3beta-hydroxysteroid dehydrogenase/isomerase family provide markers for subclassification of human primary aldosteronism. J Clin Endocrinol Metab *99*, E257-262.
4. Doi, M., Takahashi, Y., Komatsu, R., Yamazaki, F., Yamada, H., Haraguchi, S., Emoto, N., Okuno, Y., Tsujimoto, G., Kanematsu, A., et al. (2010). Salt-sensitive hypertension in circadian clock-deficient Cry-null mice involves dysregulated adrenal Hsd3b6. Nat Med *16*, 67-74.
5. Ota, T., Doi, M., Yamazaki, F., Yarimizu, D., Okada, K., Murai, I., Hayashi, H., Kunisue, S., Nakagawa, Y., and Okamura, H. (2014). Angiotensin II triggers expression of the adrenal gland zona

glomerulosa-specific 3beta-hydroxysteroid dehydrogenase isoenzyme through de novo protein synthesis of the orphan nuclear receptors NGFIB and NURR1. Mol. Cell. Biol. *34*, 3880-3894.

6. Hattangady, N.G., Olala, L.O., Bollag, W.B., and Rainey, W.E. (2012). Acute and chronic regulation of aldosterone production. Mol. Cell. Endocrinol. *350*, 151-162.

7. Clyne, C.D., Zhang, Y., Slutsker, L., Mathis, J.M., White, P.C., and Rainey, W.E. (1997). Angiotensin II and potassium regulate human CYP11B2 transcription through common cis-elements. Mol. Endocrinol. *11*, 638-649.

8. Nogueira, E.F., and Rainey, W.E. (2010). Regulation of aldosterone synthase by activator transcription factor/cAMP response element-binding protein family members. Endocrinology *151*, 1060-1070.

9. Bird, I.M., Mathis, J.M., Mason, J.I., and Rainey, W.E. (1995). Ca(2+)-regulated expression of steroid hydroxylases in H295R human adrenocortical cells. Endocrinology *136*, 5677-5684.

10. Bassett, M.H., Suzuki, T., Sasano, H., De Vries, C.J., Jimenez, P.T., Carr, B.R., and Rainey, W.E. (2004). The orphan nuclear receptor NGFIB regulates transcription of 3beta-hydroxysteroid dehydrogenase. implications for the control of adrenal functional zonation. J Biol Chem *279*, 37622-37630.

11. Bird, I.M., Imaishi, K., Pasquarette, M.M., Rainey, W.E., and Mason, J.I. (1996). Regulation of 3 beta-hydroxysteroid dehydrogenase expression in human adrenocortical H295R cells. J Endocrinol *150 Suppl*, S165-173.

12. Bassett, M.H., White, P.C., and Rainey, W.E. (2004). The regulation of aldosterone synthase expression. Mol. Cell. Endocrinol. *217*, 67-74.

13. Nicol, M.R., Papacleovoulou, G., Evans, D.B., Penning, T.M., Strachan, M.W., Advani, A., Johnson, S.J., Quinton, R., and Mason, J.I. (2009). Estrogen biosynthesis in human H295 adrenocortical carcinoma cells. Mol. Cell. Endocrinol. *300*, 115-120.

14. Maglich, J.M., Kuhn, M., Chapin, R.E., and Pletcher, M.T. (2014). More than just hormones: H295R cells as predictors of reproductive toxicity. Reprod. Toxicol. *45*, 77-86.

15. Oskarsson, A., Ulleras, E., Plant, K.E., Hinson, J.P., and Goldfarb, P.S. (2006). Steroidogenic gene expression in H295R cells and the human adrenal gland: adrenotoxic effects of lindane in vitro. J Appl Toxicol *26*, 484-492.

16. Hilscherova, K., Jones, P.D., Gracia, T., Newsted, J.L., Zhang, X., Sanderson, J.T., Yu, R.M., Wu, R.S., and Giesy, J.P. (2004). Assessment of the effects of chemicals on the expression of ten steroidogenic genes in the H295R cell line using real-time PCR.

Toxicol Sci *81*, 78-89.

17. Bassett, M.H., Zhang, Y., White, P.C., and Rainey, W.E. (2000). Regulation of human CYP11B2 and CYP11B1: comparing the role of the common CRE/Ad1 element. Endocr Res *26*, 941-951.

18. Nogueira, E.F., Vargas, C.A., Otis, M., Gallo-Payet, N., Bollag, W.B., and Rainey, W.E. (2007). Angiotensin-II acute regulation of rapid response genes in human, bovine, and rat adrenocortical cells. J Mol Endocrinol *39*, 365-374.

19. Romero, D.G., Plonczynski, M., Vergara, G.R., Gomez-Sanchez, E.P., and Gomez-Sanchez, C.E. (2004). Angiotensin II early regulated genes in H295R human adrenocortical cells. Physiol. Genomics *19*, 106-116.

20. Bassett, M.H., Suzuki, T., Sasano, H., White, P.C., and Rainey, W.E. (2004). The orphan nuclear receptors NURR1 and NGFIB regulate adrenal aldosterone production. Mol. Endocrinol. *18*, 279-290.

21. Romero, D.G., Rilli, S., Plonczynski, M.W., Yanes, L.L., Zhou, M.Y., Gomez-Sanchez, E.P., and Gomez-Sanchez, C.E. (2007). Adrenal transcription regulatory genes modulated by angiotensin II and their role in steroidogenesis. Physiol. Genomics *30*, 26-34.

22. Wang, T., and Rainey, W.E. (2012). Human adrenocortical carcinoma cell lines. Mol. Cell. Endocrinol. *351*, 58-65.

Chapter 2

Age-associated pathogenesis of dry eye disease involves an attenuation of circadian clock-regulated 3β-HSD activity in the meibomian glands

Introduction

In mammals, behavior, physiology and metabolism are subjected to a well-controlled daily rhythm, generated by an internal self-sustained molecular oscillator referred to as the circadian clock [1-3]. Although it is well known that malfunction of the circadian clock is linked to the pathogenesis of a wide variety of disease [4-6], it is unclear whether it affects the development of dry eye disease.

Dry eye disease is a multifactorial disorder of the ocular surface characterized by a loss of the homeostasis of the tear film due to tear deficiency or excessive tear evaporation, which induces damage to the ocular surface and is associated with symptoms of ocular discomfort. Dry eye disease is classified into two types: aqueous-deficient and evaporative dry eye. The former is due to decreased tear secretion from the lacrimal gland, whereas the latter is caused primarily by meibomian gland dysfunction (MGD). Meibomian glands are holocrine glands embedded in the eyelid and secrete lipid onto the ocular surface tear film to reduce aqueous tear evaporation. Thus, the impediment of the meibomian gland function leads to evaporative dry eye, which is the most common form of dry eye disease in both clinic and population based studies [7, 8]. However, molecular basis of MGD remains largely to be defined. Although aging is one of the major risk factors for dry eye [9-11], the underlying mechanism(s) remains totally unknown.

Sex steroids, such as androgens and estrogens, strongly affect the meibomian gland function [12, 13]. In particular, the androgen testosterone has been reported to be associated with the development of age-associated dry eye disease. Testosterone has an ability to enhance the meibomian gland functions, including cell differentiation, cell proliferation, and lipogenesis in the meibocyte [14-16]. It is conceivable that aging-induced reduction of testosterone production could be a potential mechanism for the development of MGD [17, 18]. However, nothing is known about the molecular mechanism(s) regulating testosterone levels within the meibomian gland.

The synthesis of sex steroids comprises processes by which cholesterol is converted to biologically active steroid hormones [19]]. The enzyme 3β-hydroxysteroid dehydrogenase/Δ^5-Δ^4-isomerase (3β-HSD) enzyme is essential for the biosynthesis of all active steroid hormones, such as those produced in the adrenal gland, testis, ovary, skin and placenta. In the present study, I focused on a role of the 3β-HSD activity within the meibomian gland.

In the present study, I found that mouse 3β-HSD isozyme Hsd3b6 is specifically expressed in acinar cells of the meibomian gland and is the sole enzyme responsible for the local steroidogenesis within the meibomian gland. Moreover, I show that circadian clock system exists in the meibomian gland and regulates meibomian Hsd3b6 enzymatic activity.

Notably, genetic ablation of *Hsd3b6* leads to the development of MGD and dry eye disease. I will also show that circadian clock malfunction and aging both lead to reduced 3β-HSD activity and thereby induce MGD-associated evaporative dry eye disease.

Materials and Methods

Creation of *Hsd3b6* knockout mice

Hsd3b6$^{-/-}$ mice were generated in the RIKEN CDB (Kobe, Japan). To generate floxed mutants for *Hsd3b6*, I constructed a targeted allele harboring the loxP-flanked exon 2 of *Hsd3b6* and an Frt-flanked neomycin resistant cassette (neo-cassette). The targeted allele was introduced into the TT2 embryonic stem cells by electroporation as described previously [20]. To delete the neo-cassette, mice were mated with *CAG-FLPe* transgenic mice (RBRC01834, RIKEN BRC). For experiments using *Hsd3b6* null mutants, I crossed *Hsd3b6* floxed mutants to *CAG-Cre* transgenic mice (RBRC01828, RIKEN BRC). Germline transmission was verified by PCR as well as Southern blotting on tail DNA.

Animal experiments

All animal studies were performed with protocols approved by the animal experimentation committee of Kyoto University. I used C57BL6 wild-type (young, 6-15 weeks old; aged, 48-96 weeks old), *Hsd3b6*$^{-/-}$, and *Bmal1*$^{-/-}$ [21] mice. Before experiments all animals were acclimated for at least 2 weeks in a 12-h light-dark cycle. For experiments in constant darkness (DD) conditions, animals were transferred to DD. Twelve hours after DD, tissues were collected at each selected time points. Where specified,

animals were maintained under desiccating conditions, in which mice were kept in 15-25% air humidity with repeated air circulation every 2 hours for 10 consecutive days. Control mice were housed in 40-60% humidity.

Whole-mount staining of meibomian glands

Whole-mount staining of meibomian glands was performed according to a previously established method [22] with modifications. The skins including the eyelids removed from mice were fixed with 4% paraformaldehyde at 4°C for 24 h and then transferred into 50% ethanol for 10 min and 70% ethanol for 20 min at room temperature. The specimens were stained with Sudan IV-saturated 70% ethanol containing and 2% NaOH for 24 h and then rinsed in 70% ethanol until excess stain was washed out completely. For the clearing of eyelids, the specimens were immersed in 25% N,N,N',N'-Tetrakis-(2-hydroxypropyl)ethylenediamine (Tokyo Chemical Industry) in glycerol for 24 h at room temperature and the unstained regions were decolorized. Before being mounted in glycerin jelly, the lateral canthi of the eyes were cut open to make the specimens flat, and the connective tissues and the debris were removed under a stereomicroscope.

Corneal fluorescein staining

Corneal fluorescein staining was performed according to a previously

established method [23] with modifications. Corneal epithelial defect was evaluated at baseline (3 days before desiccating condition) and under acute desiccated condition. To desiccate murine ocular surface, the mice were exposed to low humidity (15-25%) without blinking for 1 h after anesthesia. 10 μL of 1% liquid sodium fluorescein (Novartis Pharma.) was instilled onto the ocular surface. Corneas were rinsed with saline and photographed with a slit lamp biomicroscope (SL 130; Carl Zeiss) under cobalt blue light 2 minutes after fluorescein instillation. Corneal punctate staining areas were scored in a blinded fashion with a grading system of 0 to 4 as follows: Grade 0, absent; 1, about 12.5% staining of the ocular surface; 2, about 25% staining of the ocular surface; 3, about 50% staining of the ocular surface; 4, about 100% staining of the ocular surface.

Assessment of tear volume

Phenol red thread tear test was performed as described [24]. I used phenol red-impregnated cotton threads (Zone-quick; Ayumi Pharma.). The threads were held with jeweler forceps and applied in the ocular surface in the lateral canthus for 60 seconds. Wetting of the thread was measured in millimeters, using the scale on the cotton thread.

Immunohistochemistry

The eyelids fixed with 4% paraformaldehyde were embedded in paraffin-wax with routine protocol. Four-micrometer-thick sections were cut on a microtome and deparaffinized with xylene and ethanol. For anti-Hsd3b6 immunohistochemistry, sections were antigen-retrieved by pressure cooking in Tris–EDTA buffer (pH 9.0) for 5 min as described elsewhere [25]. Sections were then immersed in PBS containing 0.1% Tween20 and incubated with anti-Hsd3b6 antibody (final concentration, 0.6 μg/mL [26]) for 24 h at 4°C. The immunoreactivities were visualized with 3,3-diaminobenzidine (DAB: brown staining) using horseradish peroxidase-labeled anti-rabbit IgG polymers (Dako, EnVision^{+} System－HRP Labelled Polymer Anti-Rabbit) according to the manufacture's protocol. After color development, sections were dehydrated and mounted, and images were taken under a light-field microscope. For detecting mPER2 immunoreactivity, sections were antigen-retrieved by pressure cooking in 10 mM sodium citrate buffer (pH 6.0) for 3.5 min. Sections were then immersed in PBS containing 0.2% Triton X-100 and blocked with 5% BSA and 5% FBS in PBS for 1 h. After incubation with anti-mPER2 antibody (1:500 dilution; PER21-A, Alpha Diagnostic) for 24 h at 4°C, the immunoreactivities were visualized with Alexa594-conjugated anti-rabbit IgG (1:500 dilution; Invitrogen). Sections were mounted in Prolong® Gold antifade reagent with DAPI (Invitrogen). After

immunofluorescent staining, sections were counterstained with hematoxylin and eosin (HE).

Laser Microdissection (LMD)

Cryosections (20 μm thick) of fresh-frozen eyelids were prepared using a cryostat (Leica) at −14°C and mounted on POL-membrane slides (Leica). For quantitative RT-PCR, sections were fixed for 2 min in an ice-cold mixture of ethanol and acetic acid (19:1), rinsed briefly in ice-cold water, stained for 45 sec in ice-cold water containing 0.05% toluidine blue, followed by two brief washes in ice-cold water (all the solutions were RNase-free). After wiping off excess water, slides were quickly air dried for 1−2 min at room temperature. As soon as moistures in the sections decreased enough for laser-cutting, cells in the meibomian glands were microdissected using a LMD6000 device (Leica) and lysed into Trizol reagent (Invitrogen). For the measurement of NAD^+ metabolites in the meibomian glands by LC/MS/MS, sections were fixed for 30 sec in ice-cold 50% ethanol, stained for 30 sec in ice-cold water containing 0.05% toluidine blue, followed by a brief wash in ice-cold 50% ethanol. After wiping off excess water, slides were quickly air dried for 1−2 min at room temperature. As soon as moistures in the sections decreased enough for laser-cutting, cells in the meibomian glands were microdissected and lysed into 50% methanol.

RNA extraction and quantitative reverse transcription-PCR (qRT-PCR)

RNA was extracted using an RNeasy micro kit (Qiagen) according to the manufacturer's protocol. Total RNA was converted to cDNA with SuperScript VILO cDNA synthesis kit (Invitrogen). Quantitative PCR analysis of individual cDNAs was achieved using THUNDERBIRD SYBR qPCR Mix (TOYOBO) with StepOnePlus real-time PCR monitoring system (Applied Biosystems). Data were normalized to a housekeeping gene, *Rplp0*. The sequences for the primers are shown in Table 1.

qRT-PCR Screen with Fluidigm Dynamic Arrays

TaqMan qPCR analysis was performed on a BioMark HD System (Fluidigm), using a 48.48 Fluidigm BioMark Dynamic Array chip (Fluidigm) according to the manufacturer's instructions. cDNA was pre-amplified for 14 cycles with a set of primers specific to the target genes (see below). Pre-amplified mixtures (total 24 samples: 6 time points × quadruplicate) were combined with a set of TaqMan probes and primers (total 32 sets: 16 genes × duplicate) on a 48.48 chip using an IFC-MX-I Controller (Fluidigm). PCR was run on a BioMark real-time reader (Fluidigm). Ct values were obtained with the Fluidigm Real-Time PCR Analysis software (Fluidigm). ΔCt was calculated by subtracting the Ct

values of *Rplp0* from the Ct values of the gene of interest. TaqMan probe and primer sets are shown in Table 2.

Detection of 3β-HSD activity in meibomian gland

3β-HSD enzymatic activities were determined by measuring the conversion of [1,2,6,7-^{3}H]-dehydroepiandrosterone (^{3}H-DHEA; PerkinElmer) to ^{3}H-androstenedione. Meibomian glands were isolated from eyelids by removing epidermis under a stereomicroscope, and cut into slices (200 μm thickness) with a tissue chopper (Mcilwain Laboratory Co.). I placed these fresh slices in 200 μL of HBSS (Invitrogen), aerated with 5% CO_2, 95% O_2 at 37°C, followed by administration of the reagent mixture (^{3}H-DHEA, final 40 nM; Dutasteride (Cayman), final 10 μM; Fadrozole hydrochloride (Sigma), final 10 μM, 4% propylene glycol). 5α-reductase blocker Dutasteride and aromatase blocker Fadrozole hydrochloride are inhibitors of steroidogenesis following androstenedione synthesis. After incubation for 30 min at 37°C without CO_2, I stopped the reaction by adding ethyl acetate. The extraction of steroids was done as previously described [4]. Eluates were subjected to HPLC-scintillation analyzer (Waters 2795 HPLC separation module, Waters; Radiomatic 625R, PerkinElmer) and separated using a LiChrospher 100 RP-18 column (4.0 mm × 250 mm, 5 μm particle size; Kanto Chemical Industry) maintained at 40°C. Mobile phase was water (buffer A) and acetonitrile (buffer B). The HPLC was run at a flow

rate of 0.7 mL/min with a linear gradient of 40-50% buffer B from 0-30 min, an isocratic elution of 30% buffer A/70% buffer B from 30-35 min, an isocratic elution of 100% buffer B from 35-40 min, and a linear gradient to 60% buffer A/40% buffer B from 40-50 min. I fractionated the eluate every minute from 0 to 40 min and counted ^{3}H radioactivity in a flow scintillation analyzer.

Detection of 3β-HSD activity with microsome fraction prepared from meibomian gland

Meibomian glands were isolated from eyelids by removing epidermis under a stereomicroscope, and were homogenized in ice-cold D-PBS containing 2×cOmplete Protease inhibitor cocktail (Roche diagnostics) and 1 mM phenylmethylsulfonyl fluoride (PMSF). After centrifugation at 700 × *g* for 10 min to remove nuclei and debris, the supernatant was ultracentrifuged at 106,000 × *g* for 1 h at 4°C. Then, the pellet (microsomal fraction) was resuspended in ice-cold D-PBS containing 2×cOmplete Protease inhibitor cocktail and 1 mM PMSF. The protein content was determined with a Bradford assay kit (Nacalai Tesque). I incubated 5 μg protein in reaction buffer (10 mM phosphate, pH 7.5, 140 mM NaCl, 4% propylene glycol) containing 100 nM ^{3}H-DHEA and 240 μM NAD^{+} for 1 h at 37°C. Where specified, I varied the NAD^{+} concentrations from 240 nM to 2400 μM. After incubation, the reaction was stopped by adding ethyl acetate. The

extraction of steroids and the measurement of 3β-HSD activity were done as described above.

Detection of 3β-HSD activity in cultured H295R cells

Human adrenocortical H295R cells (ATCC CRL-2128) were cultured in DMEM/F-12 medium (Invitrogen) supplemented with 2.5% Nu serum (BD Biosciences) and 1% ITS premix (BD Biosciences). The cells were plated on 24-well plates (2×10^5 cells per well) and cultured for three days prior to ^{3}H-DHEA treatment. Where specified, the NAMPT blocker FK866 (final concentration, 10 nM; Cayman) was added either alone or together with β-nicotinamide mononucleotide (final concentration, 100 μM; Sigma) were added to the culture medium 24 h prior to 3β-HSD assays. After incubation with 40 nM ^{3}H-DHEA for 1 h at 37°C without CO_2, I collected culture medium and stopped the reaction by adding ethyl acetate. The extraction of steroids and the measurement of 3β-HSD activity were done as described above.

NAD^+ measurement by LC-UV

NAD^+ levels in H295R cells were measured with a published method using a Shimadzu HPLC instrument (LC-20AT Quaternary Solvent Delivery Unit, SPD-20A UV detector, SIL-20A Autosampler, DGU-20A5 Degasser)

[27]. For the extraction of NAD^+, samples were homogenized in ice-cold 10% perchloric acid followed by centrifugation, supernatants were neutralized with ice-cold 3M K_2CO_3. After removal of salt precipitants, the extracts were filtered with 0.22 μm hydrophilic nylon filter (Starlab Scientific) and loaded on a HPLC column (COSMOSIL Packed Column 5C18-PAQ, 4.6 mm I.D. × 150 mm, 5 μm particle size; Nacalai Tesque). Mobile phase was water containing 0.05 M phosphate buffer (buffer A) and methanol (buffer B). The HPLC was run at a flow rate of 1 mL/min with 100% buffer A from 0-3 min, a linear gradient to 95% buffer A/5% buffer B from 3-4 min, 95% buffer A/5% buffer B from 4-9 min, a linear gradient to 85% buffer A/15% buffer B from 9-11 min, 85% buffer A/15% buffer B from 11-21 min, and a linear gradient to 100% buffer A from 21-22 min. NAD^+ levels were quantitated based on the peak area compared to a standard curve and normalized to weights of tissues or the total volume of cells.

Mass Spectrometry (LC-MS/MS) analysis of NAD^+ metabolites in the meibomian glands

Liquid chromatography-tandem mass spectrometry (LC-MS/MS) was performed with a Shimadzu Nexera UHPLC/HPLC System (Shimadzu) coupled to a LCMS-8040 triple quadrupole mass spectrometer (Shimadzu) in the positive mode. Using laser-microdissection, the meibomian glands

were selectively isolated into 50% methanol. Then, the samples were mixed with chloroform (1:1) and sonicated 15 times for 30 sec each time using a Bioruptor UCW-201TM apparatus (Tosho Denki). Following centrifugation, supernatants were filtered with 0.22 μm hydrophilic nylon filter and freeze-dried with a freeze vacuum dryer (FDU-2110; EYELA). Samples were redissolved in distilled water before analysis and separated through a COSMOSIL Packed Column 5C18-PAQ (2.0 mm I.D. × 150 mm, 5 μm particle size; Nacalai Tesque). Mobile phase was water containing 0.05% formic acid (buffer A) and methanol containing 0.05% formic acid (buffer B). The LC was run at a flow rate of 0.2 mL/min with 100% buffer A from 0-3 min, a linear gradient to 95% buffer A/5% buffer B from 3-4 min, 95% buffer A/5% buffer B from 4-9 min, a linear gradient to 85% buffer A/15% buffer B from 9-11 min, 85% buffer A/15% buffer B from 11-21 min, and a linear gradient to 25% buffer A/75% buffer B from 21-22 min, 25% buffer A/75% buffer B from 22-27 min. Injection volume was 10 μL. NAD^+ metabolites was detected using the multiple reaction monitoring mode and identified by comparison of their LC retention times and MS^2 fragmentation patterns with those of authentic standards. Their levels were quantified based on the peak area compared to a standard curve and normalized to the area of meibomian gland sections captured by LMD. Each optimal MS/MS transition was selected as follows: NAD^+, m/z 663.85>136.05; NMN, 334.85>123.05; NAM, 124.30>80.05; NR,

254.90>123.10; NA, 122.75>80.05.

SDS-PAGE-based Immunoblotting

Immunoblot for Per2, Nurr1, Nor1, and α-tubulin were performed as described [28] with modifications. Meibomian glands were isolated from eyelids by removing epidermis under a stereomicroscope. Then tissues were minced into pieces and lysed with 2× Laemmli sample buffer containing 2× cOmplete Protease inhibitor cocktail (Roche diagnostics) and 2× PhosSTOP phosphatase inhibitor cocktail (Roche diagnostics). After centrifugation at 12,000 × *g* for 12 min, supernatant proteins were subjected to Immunoblot analysis. For Per2 detection, proteins were separated by electrophoresis through sodium dodecyl sulfate (SDS)-6% polyacrylamide (120:1, acrylamide:bis-acrylmide) gels, and immunoblotted with the PER2 antibody (final concentration, 0.4 ng/mL [29]). For detection of other proteins, proteins were separated by electrophoresis through a 7.5% polyacrylamide gel (E-R7.5L; ATTO), and immunoblotted with Nurr1 (1:1000 dilution; N1404 antibody; Perseus Proteomics), Nor1 (1:500 dilution; H7833 antibody; Perseus Proteomics), or α-tubulin (1:2000 dilution; T6199 antibody; Sigma).

Blue native PAGE-based immunodetection of Hsd3b6

Meibomian glands were homogenized in ice-cold 50 mM Tris-HCl (pH 7.2) buffer containing 1 × cOmplete Protease inhibitor cocktail and 1 mM DTT, followed by ultracentrifugation at 106,000 × *g* for 1 h at 4°C. The pellet was then resuspended in 1 × NativePAGE™ Sample Buffer (Thermo) containing 1% digitonin, 1 × cOmplete Protease inhibitor cocktail, and 1 mM DTT. Before loading samples on the NativePAGE™ Novex® Bis-Tris Gel (Thermo), the NativePAGE™ 5% G-250 Sample Additive (Thermo) was added to the loading samples. Electrophoresis was performed using NativePAGE™ Running Buffer (Thermo) and NativePAGE™ Cathode Additive (Thermo) according to the manufacturer's protocol at a constant current of 1 mA at 4°C. Proteins in the gel were electroblotted to a polyvinylidene difluoride membrane (Clear Blot Membrane-P plus, ATTO) with a blotting buffer containing 25 mM Tris, 200 mM Glycine, 10% methanol, and 1× NativePAGE™ Cathode Additive at a constant current of 350 mA for 1.5 h. After incubation with a blocking buffer (Blocking One, Nacalai Tesque) for 30 min at room temperature, the blots were further incubated with PBS containing 0.05% Tween 20 for more than 24 h to remove CBB on the blots. The blots were incubated with anti-Hsd3b6 antibody (final concentration, 0.6 μg/mL [26]), and the immunoreactivities were visualized using a horseradish peroxidase-labeled anti-rabbit IgG polymers along with ECL™ Prime

Western Blotting Detection reagent (GE Healthcare).

Statistical analysis

I used two-tailed Student's *t* test for the comparison of two test groups. To assess the difference of the size of meibomian glands between WT and *Hsd3b6*$^{-/-}$ mice, I used two-way ANOVA with Bonferroni *post hoc* test. Pair wise comparison of corneal fluorescein staining scores was analyzed with three-way ANOVA with Sidak *post hoc* test. Circadian oscillations of 3β-HSD enzymatic activity were assessed using the non-parametric JTK-Cycle algorithm [30].

Table 1 Primer sequences for qRT-PCR

	RefSeq	Forward (5'→3')	Reverse (5'→3')
Hsd3b6	NM_013821	TGATGGGAAGAGGGTGGAG	AGGTGCTGAGAGGCTTGGA
Per2	NM_011066	CCATCCACAAGAAGATCCTAC	GCTCCACGGGTTGATGAGC
Bmal1	NM_007489	CCTAATTCTCAGGGCAGCAGAT	TCCAGTCTTGGCATCAATGAGT
Dbp	NM_016974	AATGACCTTTGAACCTGATCCCGCT	GCTCCAGTACTTCTCATCCTTCTGT
E4bp4	NM_017373	CACGGACCAGGGAGCAGAAC	CGGATGGAGGAGACAAATCAC
Nurr1	NM_013613	GCACTTCGGCGGAGTTG	GGAATCCAGCCCGTCAGA
Nor1	NM_015743	AGTGTCGGGATGGTTAAGGAA	ACGACCTCTCCTCCCTTTCA
Rplp0	NM_007475	CTCACTGAGATTCGGGATATG	CTCCCACCTTGTCTCCAGTC

Table2 Primer and probe sequences for qRT-PCR Screen with Fluidigm Dynamic Arrays

	RefSeq	Forward primer (5'-3')	Reverse primer (5'-3')	Probe (5'-3')
Per1	NM_011065	CAGGCTTCGTGGACTTGAGC	AGTGGTGTCGGCGACCAG	6-FAM-AGCCCCTGGCTGCCATGG-TAMRA
Per2	NM_011066	GCACATCTGGCACATCTCGG	TGGCATCACTGTTCTGAGTGTC	6-FAM-AGGCACCTCCAACATGCAACGAGCC-TAMRA
Per3	NM_011067	ACAGCTCTACATCGAGTCCATG	CAGTGTCTGAGAGGAAGAAAAGTC	6-FAM-TTCTGCTCATCACCACCCTGCGGTTCC-TAMRA
Cry1	NM_007771	TAGCCAGACACGCGGTTG	AGCAGTAACTCTTCAAAGACCTTCA	6-FAM-TGATCCACAGGTCACCACGAGTCAGGAA-TAMRA
Cry2	NM_009963	TGGACAAGCACTTGGAACGG	GGCCAGTAAGGAATTGGCATTC	6-FAM-AGGTCTCTCATAGTTGGCAACCCAGGC-TAMRA
Clock	NM_007715	TGGCATTGAAGAGTCTCTTCCTG	GAGACTCACTGTGTTGATACGATTG	6-FAM-ACCCAGAATCTTGGCTTTTGTCAGCAGC-TAMRA
Npas2	NM_008719	CCAGCCCATCCAGCCTATGA	GCTGTTGGTAGGGTGTGAGTC	6-FAM-TGGCTCTGTGCATACTTGACTTGCCGTC-TAMRA
Arntl1	NM_007489	GTACGTTTCTCGACACGCAATAG	GTACCTAGAAGTTCCTGTGGTAGA	6-FAM-CGCCAAAATAGCTGTCGCCCTCTGATCT-TAMRA
Arntl2	NM_172309	AGCACTGAACCCGCCCAC	GCAGCCATGTCTATGCTGTCA	6-FAM-ACCACTTCCCGGTGACAGTGCCCA-TAMRA
Dbp	NM_016974	CGGCTCTTGCAGCTCCTC	GTGTCCCTAGATGTCAAGCCTG	6-FAM-CGGCTCCCAGAGTGGCCCGC-TAMRA
Nfil3	NM_017373	CGCCAGCCCCGGTTACAG	CATCCATCAATGGGTCCTTCTG	6-FAM-CAGGGAGCAGAACCACGATAACCCATGA-TAMRA
Rora	AK035351	GAGAGACTTCCCCAACCGTG	CTGGCAGGTTTCCAGGTGG	6-FAM-TGGCAGAACTAGAACACCTTGCCCAGAA-TAMRA
Nr1d1	NM_145434	TCAGCTGGTGAAGACATGACG	GAGGAGCCACTAGAGCCAATG	6-FAM-CCCTGGACTCCAATAACAACACAGGTGG-TAMRA
Bhlhe40	NM_011498	AGCGGTTTACAAGCTGGTGAT	GGTCCCGAGTGTTCTCATGC	6-FAM-CCTCACGGGCACAAGTCTGGAAACCTG-TAMRA
Bhlhe41	NM_024469	ACATCTGAAATTGACAACACTGGG	GCGCTCCCCATTCTGTAAAG	6-FAM-TCTTCTGATGCTGCTGCTCAGTTAAGGC-TAMRA
Rplp0	NM_007475	GCGTCCTCGTTGGAGTGAC	AAGTAGTTGGACTTCCAGGTCG	6-FAM-TGGCAATCCCTGACGCACCGCC-TAMRA

Results

Molecular circadian clock in the mouse meibomian glands.

To test the possibility that the meibomian glands contain a molecular clock system, I examined immunolocalization of the mammalian core clock protein Period2 (Per2) in the meibomian gland at two different circadian time (CT) points, CT8 and CT20 (CT0 denotes the beginning of the subjective day and CT12 the beginning of the subjective night) under constant dark (DD) conditions. I found intensed immunolocalization of Per2 in the nuclei of the meibomian gland acinar cells at CT20. In contrast, Per2 was almost undetectable at CT8, indicating temporal variations of Per2 expression (**Fig. 1A**). To verify the circadian expression profiles of Per2, eyelids were sampled at 4-h intervals across 24 h in DD and subjected to western blot analysis. Consistent with the result of immunohistochemistry, Per2 expression was highest at CT20 and lowest at CT8. As reported in other tissues, Per2 proteins in the meibomian gland also displayed circadian changes in electrophoretic mobility (**Fig. 1B**), illustrating the presence of normal Per2 protein oscillations in the meibomian gland. In addition, I observed that the orphan nuclear receptors Nurr1 and Nor1, which are both known clock-controlled genes [31], also showed circadian variations in abundance (**Fig. 1B**). To test the expression profiles of the other clock genes and clock-controlled genes, I performed mRNA expression analysis using laser-microdissected meibomian gland

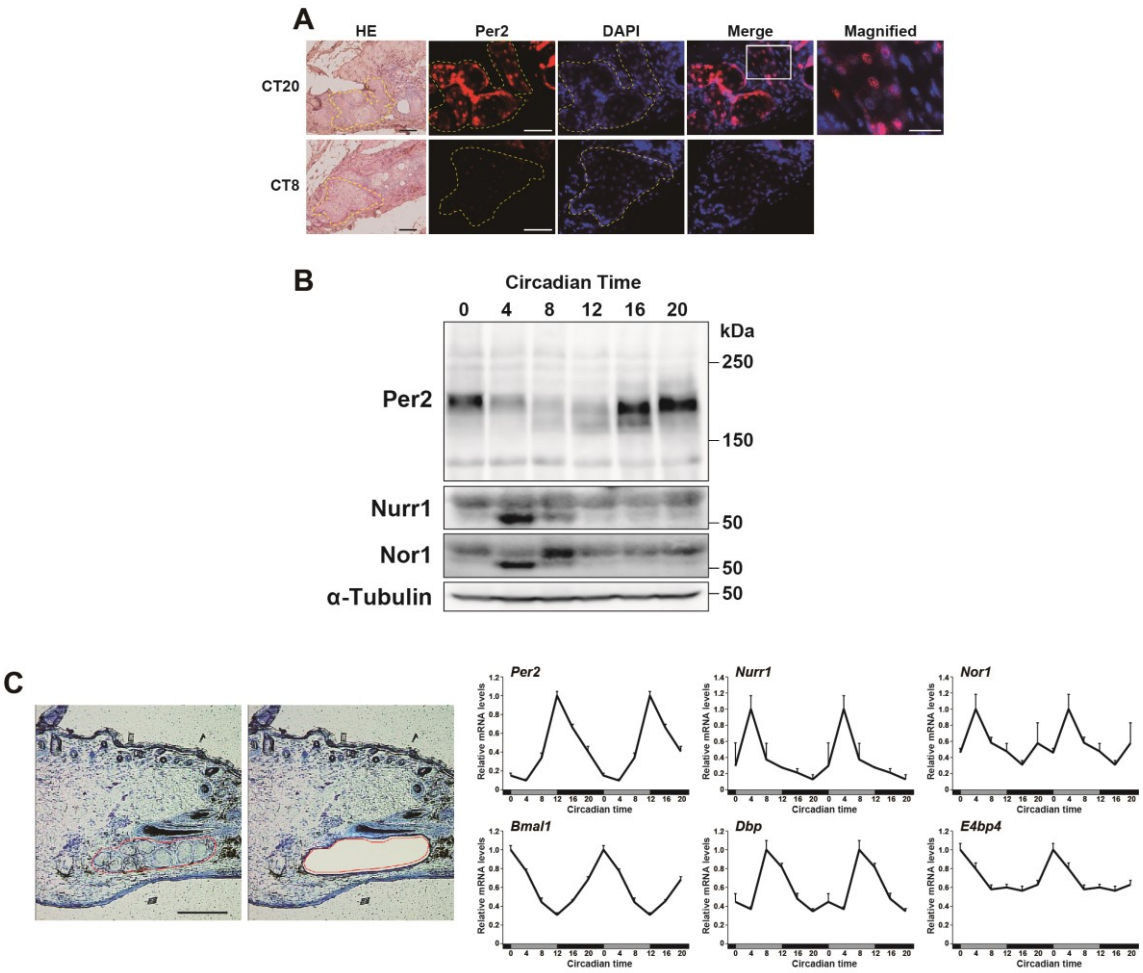

Figure 1 Circadian expression profiles of clock genes and clock-controlled genes in the mouse meibomian glands.

(A) Representative immunofluorescent images of Per2 (red) and DAPI-based nuclear staining (blue) in the meibomian glands at CT8 and CT20 in DD. Merge shows combined images for Hsd3b6 and DAPI staining. The sections were counterstained with hematoxylin and eosin (HE). Dashed lines indicate representative meibomian gland cells. White box indicates area of higher magnification view. Scale bars, 50 μm and 20 μm. (B) Immunoblots showing circadian expression profiles of Per2, Nurr1, and Nor1 in the meibomian glands of WT mice in DD. α-Tubulin was used as a loading control. (C) Circadian mRNA expression profiles of clock genes and clock-controlled genes including *Nurr1* and *Nor1* in the meibomian glands under DD conditions. Relative expression levels were determined by qRT-PCR and normalized to those of ribosomal protein large P0 (Rplp0) gene. Data are shown in double plot. Values are means ± s.e.m. (n=4 for each data point) relative to the peak time point. The micrographs show a representative tissue section stained with toluidine blue before and after laser microdissection. Red line delineates the laser-track. Scale bar, 200 μm.

cells (**Fig. 1C**). Quantitative RT-PCR analysis confirmed circadian expression of *Per2*, *Nurr1*, and *Nor1*. Furthermore, I found that the meibomian gland cells also displayed characteristic circadian mRNA expression profiles of other clock genes, such as *Bmal1*, *Dbp*, *E4bp4*, *Per1*, *Per3*, *Cry1*, *Cry2*, *Npas2*, and *Rev-erbα* (**Fig. 1C**, **Supplementary Fig. 1**). These data revealed that the robust circadian clock system exists in the mouse meibomian gland.

Identification of Hsd3b6 expression and intrinsic 3β-HSD activity in the meibomian glands.

Steroid hormones are considered to play a role in maintenance of the meibomian gland homeostasis [13]. Therefore I examined a potential involvement of the meibomian circadian clock in regulation of local steroid synthesis in the meibomian gland. To test this possibility, I focused on the 3β-hydroxysteroid dehydrogenase/Δ^5-Δ^4-isomerase (3β-HSD) enzyme family that is known to be essential for production of all active steroid hormones, such as those synthesized in the adrenal gland, testis, ovary, skin, and placenta. I found that akin to the skin sebaceous gland, the meibomian gland shows expression of the type VI 3β-HSD isozyme (Hsd3b6) (**Fig. 2A**). The gene encoding this enzyme differs from the one encoding the type I 3β-HSD (Hsd3b1), which is expressed in ovary, testis,

and adrenal fasciculata cells [26, 32]. Using Hsd3b6 subtype-specific antibody, I immunostained sagittal sections of the upper eyelid and found restricted expression of Hsd3b6 in the acinar cells of the meibomian gland (**Fig. 2A**), where Per2 exhibits overt circadian expression (**Fig. 1A**). It therefore appears likely that the meibomian gland has an intrinsic system to produce 3β-HSD activity in the cells containing the circadian clock.

To directly assess the endogenous 3β-HSD activity in the meibomian gland, I developed pulse-chase assays with freshly isolated meibomian gland tissues (**Fig. 2B**). The isolated tissues were incubated in HBSS medium in the presence of radioisotope-labelled 3β-HSD substrate ([1,2,6,7-^{3}H]-dehydroepiandrosterone; hereafter, ^{3}H-DHEA) for 30 min, and the products were assessed with an HPLC-linked scintillation counter. As shown in **Fig. 2B**, the chromatogram reveals a considerable conversion from ^{3}H-DHEA (green) to ^{3}H-androstenedione (magenta). Importantly, this converting activity was completely abolished by boiling the tissues before assay (**Fig. 2B**), demonstrating that the meibomian gland has an intrinsic 3β-HSD activity.

Circadian clock regulates meibomian 3β-HSD enzymatic activity and maintains the morphology of the meibomian gland.

The intra-tissue 3β-HSD activities in the meibomian gland might undergo

day/night variations. To test this, the meibomian glands were sampled every 6 hours over two consecutive days under normal 12-h light:12-h dark (LD) conditions, and 3β-HSD enzymatic activities were determined for each time point (**Fig. 2C**). I observed that the meibomian gland 3β-HSD activity cycled on a daily basis (**Fig. 2C**; JTK-cycle $P < 0.05$), with peaks occurring near the beginning of the rest period for mice (ZT3; ZT represents Zeitgeber time; ZT0 denotes lights-on and ZT12 lights-off). The diurnal fluctuation of the meibomian 3β-HSD activities was not produced by the circadian clock-deficient *Bmal1*$^{-/-}$ mice (**Fig. 2C**), indicating that the core clock machinery is required for the daily control of intrinsic 3β-HSD activities in the meibomian gland.

Because *Bmal1*$^{-/-}$ mice are known to show age-related pathologies [33] and MGD increases with age [34], I hypothesized that dysregulated 3β-HSD activities in the *Bmal1*$^{-/-}$ mice might be associated with MGD development. To evaluate lipid content and morphologies of the meibomian gland in the eyelids, I employed whole mount visualization of the meibomian glands using modified Sudan IV lipid staining, in which the specimens (whole eyelids) were stained and subjected to a tissue-clearing procedure before imaging with light microscopy. I quantified the area of meibomian glands and the number of meibomian ducts of WT and *Bmal1*$^{-/-}$ mice (**Fig. 2D**). Notably, *Bmal1*$^{-/-}$ male mice showed severe atrophy of meibomian glands as compared to WT mice (**Fig. 2E**), while there was no

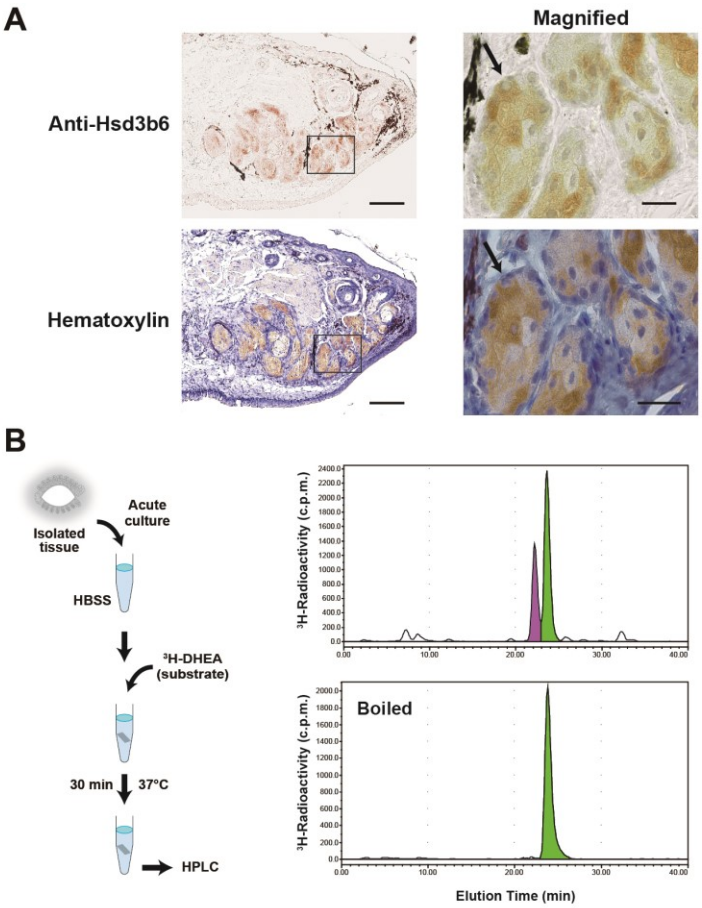

(Legend on next page)

Figure 2 Meibomian 3β-HSD enzymatic activity oscillates in a circadian fashion

(A) Representative anti-Hsd3b6 immunohistochemistry and hematoxylin staining of sagittal serial sections of upper eyelid. Black Box indicates area of higher magnification view. Arrows indicate representative nuclei of the meibomian gland acinar cells. Scale bars, 100 μm and 20 μm. (B) Experimental scheme for the measurement of endogenous 3β-HSD activity with freshly isolated meibomian gland tissues (left). Chromatograms showing endogenous 3β-HSD enzymatic activity in the meibomian gland (right). (C) Time-of-day-dependent changes in 3β-HSD enzymatic activity in the meibomian glands of WT and *Bmal1*$^{-/-}$ mice. 3β-HSD enzymatic activities were determined by measuring the conversion of ^{3}H-DHEA to ^{3}H-androstenedione. Tissues were sampled at 6-h intervals for 48 h for WT and 24 h for *Bmal1*$^{-/-}$ under LD conditions. Values are the means ± s.e.m. (n=4 for each data point). $P < 0.05$ indicates the presence of rhythm using JTK-cycle algorithm. (D–F) The morphology of the meibomian gland of WT and *Bmal1*$^{-/-}$ female mice. (D) Whole mount meibomian gland staining of upper and lower eyelids. Scale bar, 1 mm. (E) The area of meibomian glands. (F) The number of meibomian gland ducts. The meibomian glands were visualized by Sudan IV lipid staining. Values are the means ± s.e.m. Numbers on the bottom of the bars indicate the number of samples in each group. *$P <$ 0.05, two-tailed Student's *t* test.

difference in the number of meibomian ducts between WT and *Bmal1*$^{-/-}$ mice (**Fig. 2F**). These anatomical features of the meibomian gland of the *Bmal1*$^{-/-}$ mice resemble those of the human MGD.

Meibomian 3β-HSD enzymatic activity declines with age.

The prevalence of MGD-associated dry eye disease increases with age [34], I therefore next examined the effect of aging on the meibomian 3β-HSD enzymatic activity. In aged mice, 3β-HSD activity in the meibomian glands was approximately 40% lower than WT mice, indicating that 3β-HSD enzymatic activity in the meibomian gland declines with age (**Fig. 3A**). In addition, as was reported in humans, aged mice also showed marked atrophy of meibomian glands (**Fig. 3B–D**). These data provided us a reason to speculate that the reduction of the intra-tissue 3β-HSD activity might underlie the development of the atrophic morphology of the meibomian gland.

***Hsd3b6*-deficient mice show defective steroidogenesis in the meibomian glands.**

The intra-tissue 3β-HSD activity might be key to maintaining meibomian function. To determine the extent to which the specific 3β-HSD isoform Hsd3b6 contributes to the meibomian gland 3β-HSD activity, I generated

Figure 3 Meibomian 3β-HSD enzymatic activity declines with age.

(A) 3β-HSD enzymatic activity in the meibomian gland of young (12 weeks old) and aged (68 weeks old) mice. Values are the means ± s.e.m (young, n=8; aged, n=4). (B–D) The morphology of the meibomian gland of young (12–15 weeks old) and aged (48 weeks old) female mice. (B) Whole mount meibomian gland staining of upper and lower eyelids. (C) The area of meibomian glands. (D) The number of meibomian gland ducts. The meibomian glands were visualized by Sudan IV lipid staining. Values are the means ± s.e.m. Numbers on the bottom of the bars indicate the number of samples in each group. ***$P < 0.01$, two-tailed Student's *t* test.

Hsd3b6-deficient mice, in which the second exon containing the initiation codon of *Hsd3b6* gene was deleted (**Fig. 4A**). Southern blotting and genotyping PCR confirmed correct gene targeting and the deletion of the target exon of the *Hsd3b6* (**Fig. 4B–D**). Noticeably, the intra-tissue 3β-HSD activity disappeared from the meibomian gland when *Hsd3b6* was deleted (**Fig. 4E**), demonstrating that Hsd3b6 is the sole enzyme responsible for the production of the local 3β-HSD activity within the meibomian gland. Moreover, consistent with the depletion of 3β-HSD activity, the expression of Hsd3b6 in the acinar epithelial cells of the meibomian gland was completely abolished in *Hsd3b6*$^{-/-}$ mice (**Fig. 4F**).

It is still unclear whether the local 3β-HSD activity exerted by the Hsd3b6 in the meibomian gland could indeed lead to steroid production. Testosterone is a steroid hormone known to have a positive effect on the meibomian gland function. However, spatial distribution of local testosterone in the eyelid is ill-defined. I therefore visualized tissue testosterone by using MALDI-imaging mass spectrometry (**Fig. 4G**). The data, interestingly, revealed that testosterone accumulates in the basal part of the meibomian gland, where Hsd3b6 is expressed (**Fig. 4F**), suggesting a possible direct contribution of Hsd3b6 to the local production of testosterone. To further test this possibility, I measured the intra-tissue testosterone levels in the meibomian glands of WT and *Hsd3b6*$^{-/-}$ male mice by using LC-MS/MS (**Fig. 4H**). Of note, the testosterone levels in the

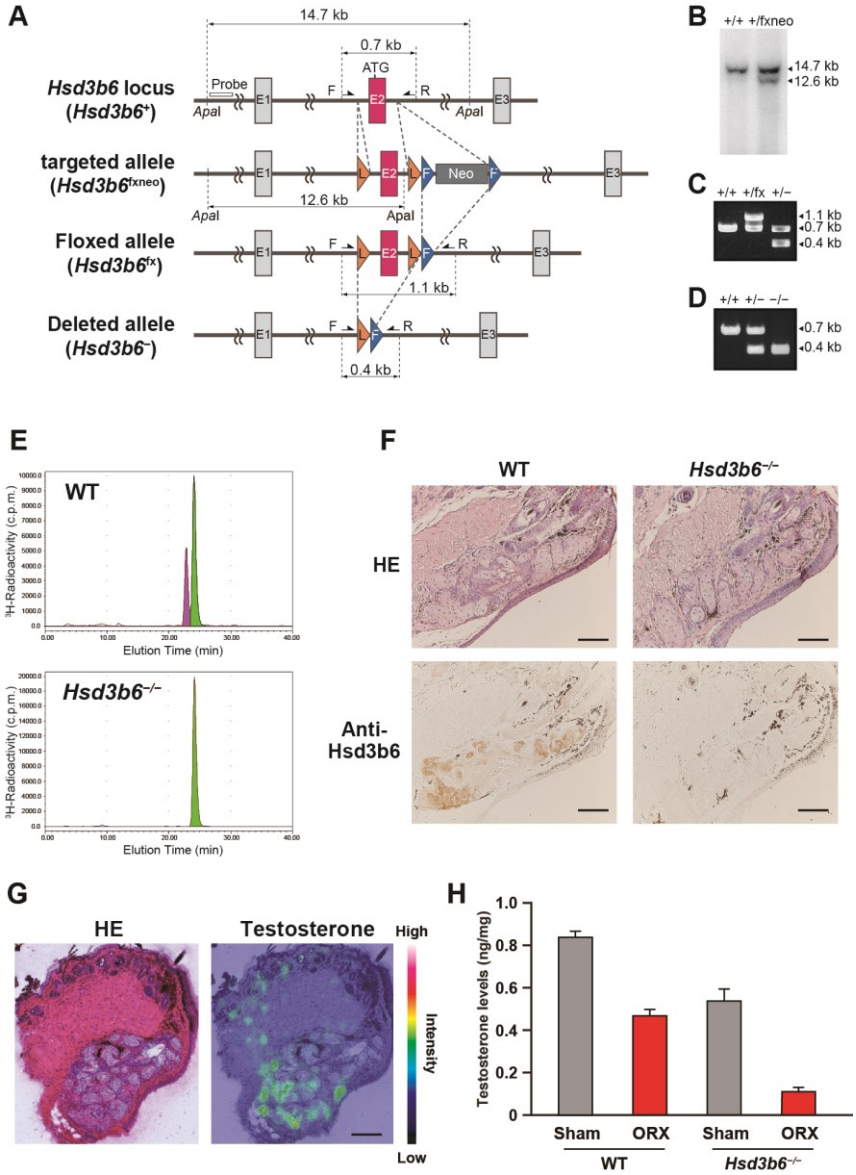

Figure 4 Hsd3b6 deficiency depletes local steroidogenesis in the meibomian glands.

(A) Schematic representation of the wild-type *Hsd3b6* locus (*Hsd3b6*$^{+}$), the targeted allele (*Hsd3b6*^{fxneo}), the floxed allele (*Hsd3b6*^{fx}), and the deleted allele (*Hsd3b6*$^{-}$). The second exon of the gene, which contains the initiation codon (ATG), was flanked with *loxP* sites. Probe used for southern blot is marked by a white box. Arrows, genotyping primers. (B) Southern blot of *Apa*I-digested DNA from *Hsd3b6*$^{+/+}$ and *Hsd3b6*$^{+/fxneo}$ mice. Genomic fragments from the wild-type (14.7 kb) and *Hsd3b6*^{fxneo} targeted (12.6 kb) alleles are indicated. (C, D) Genotyping PCRs. Amplified DNA fragments from *Hsd3b6*$^{+}$ (0.7 kb), *Hsd3b6*^{fx} (1.1 kb), and *Hsd3b6*$^{-}$ (0.4 kb) alleles are indicated. (E) 3β-HSD enzymatic activity in the meibomian glands of WT and *Hsd3b6*$^{-/-}$ mice. 3β-HSD enzymatic activities were determined by measuring the conversion of ^{3}H-DHEA (green) to ^{3}H-androstenedione (magenta). (F) Representative anti-Hsd3b6 immunohistochemistry and HE staining of serial sections from WT and *Hsd3b6*$^{-/-}$ eyelids. Scale bars, 100 μm. (G) Localization of testosterone in mouse eyelid tissue section, visualized by matrix-assisted laser desorption ionization (MALDI)-imaging mass spectrometry. The section was counterstained with HE. Scale bar, 200 μm. (H) Testosterone levels in the meibomian glands of WT and *Hsd3b6*$^{-/-}$ mice, measured by LC-MS/MS. To evaluate the degree of local steroid production, meibomian intra-tissue testosterone levels of male mice (ng per mg weight of tissue) were measured under the conditions with or without orchidectomy (ORX). Values are the means ± s.e.m. (n=2, 4).

meibomian gland of *Hsd3b6*$^{-/-}$ male mice were reduced to about 50% of those observed for the WT mice. The remaining testosterone is likely derived from the testis, because the testosterone levels in orchidectomized *Hsd3b6*$^{-/-}$ mice show further decrease to less than 15% of those of WT mice. These results indicate that local 3β-HSD activity in the meibomian gland contributes to the meibomian testosterone levels to an extent almost equivalent to that supplied by the testis.

***Hsd3b6*-deficient mice show meibomian gland atrophy leading to dry eye disease.**

To test for the physiological consequence of the deletion of local 3β-HSD activity in the meibomian gland, I examined morphologies of the meibomian gland of the *Hsd3b6*$^{-/-}$ mice. Notably, *Hsd3b6*$^{-/-}$ mice showed severe atrophy of meibomian glands compared to WT mice, while there was no difference in the number of meibomian ducts between the two genotypes (**Fig. 5A–F**). Furthermore, I found exacerbated meibomian atrophy in the *Hsd3b6*$^{-/-}$ mice when the animals were maintained under low humidity conditions, which promote the desiccation of their ocular surface. Importantly, analogous phenotypes were observed for male (**Fig. 5A–C**) and female (**Fig. 5D–F**) mice, showing that in both genders the lack of the meibomian 3β-HSD activities leads to MGD.

MGD is the most frequent cause for evaporative dry eye, raising a

question of whether the deficiency of local 3β-HSD activity leads to dry eye disease. To score the incidence of evaporative dry eye disease, corneal fluorescein staining was evaluated before (baseline) and after desiccation treatment in WT and *Hsd3b6*$^{-/-}$ mice (**Fig. 5G, J, H, K**). Minimal punctate staining on the corneal surface was recorded at baseline in both WT and *Hsd3b6*$^{-/-}$ mice. In *Hsd3b6*$^{-/-}$ mice, fluorescein scores were significantly increased after 1-h desiccation treatment compared with baseline for both male and female mice (**Fig5. H, K**; three-way ANOVA with Sidak post hoc test, $P < 0.01$ for male, $P < 0.001$ for female). By comparison, in WT mice, although there was a trend towards increased fluorescein scores post 1-h desiccation for both male and female, none of these differences reaches significance (**Fig5. H, K**). I also measured tear volumes of WT and *Hsd3b6*$^{-/-}$ mice. To do this, I performed phenol red thread tear tests (**Fig. 5I, L**). Importantly, despite displaying evaporative dry eyes, *Hsd3b6*-deficient mice beared increased tear volumes as compared to WT mice (**Fig. 5I, L**; two-tailed Student's t test, $P < 0.05$ for male, $P < 0.01$ for female), suggesting a compensatory tear production to ameliorate MGD-associated evaporative dry eye disease in *Hsd3b6*$^{-/-}$ mice. I conclude that the meibomian Hsd3b6 activity is essential to maintain meibomian gland function and that its deletion leads to MGD-associated dry eye disease.

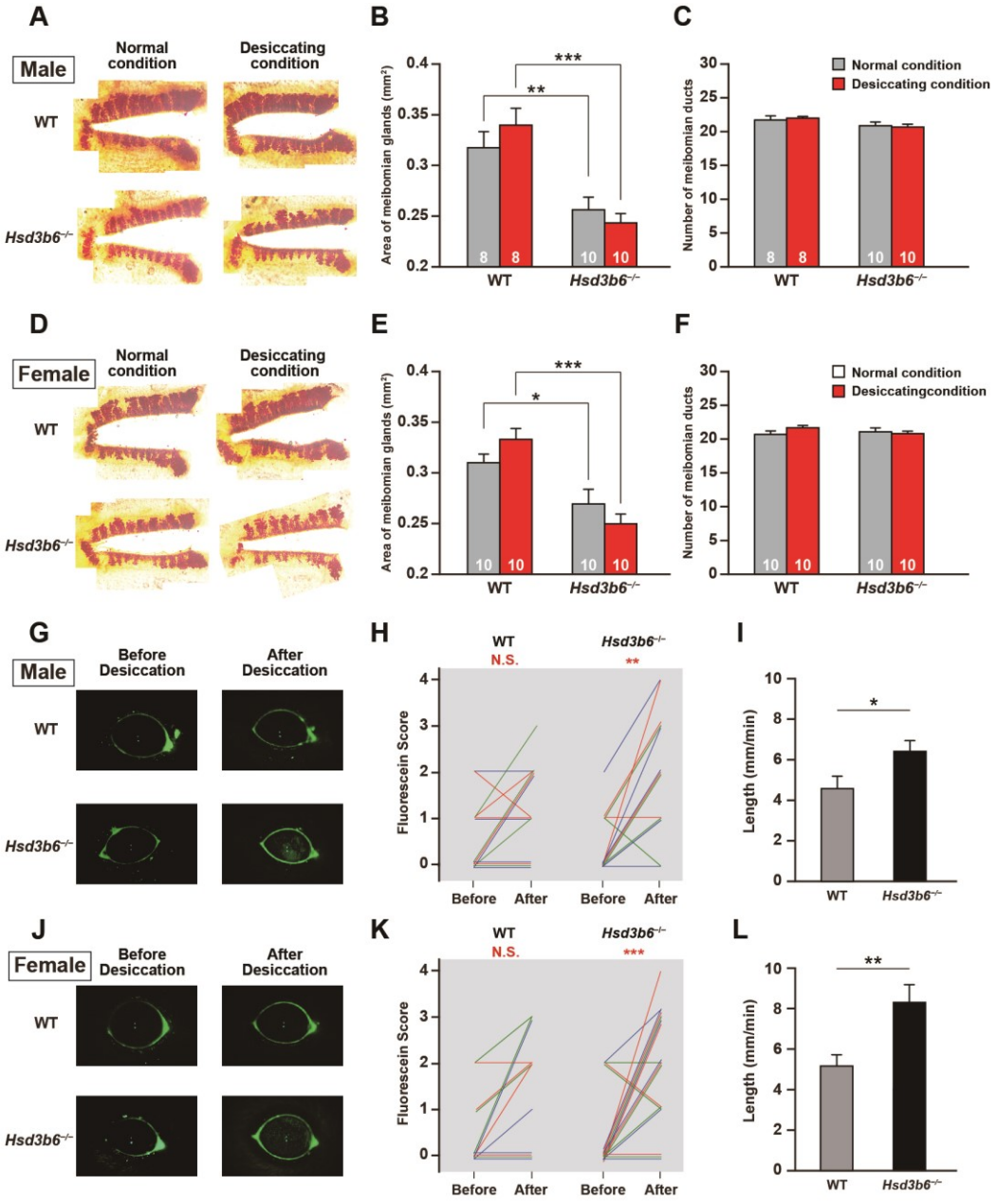

Figure 5 *Hsd3b6*-deficient male and female mice show meibomian gland atrophy and dry eye disease.
(A–F) The morphology of the meibomian gland of WT and *Hsd3b6*$^{-/-}$ mice kept under standard or low humidity conditions. (A, D) Whole mount meibomian gland staining of upper and lower eyelids. (B, E) The area of meibomian glands. (C, F) The number of meibomian gland ducts. The meibomian glands were visualized by Sudan IV lipid staining. Assays were performed with male (A–C) and female (D–F) mice. Values are the means ± s.e.m. Numbers on the bottom of the bars indicate the number of samples in each group. **P* < 0.05; ***P* < 0.01; ****P* < 0.001, two-way ANOVA with Bonferroni *post hoc* test. (G–L) Evaporative dry-eye test for WT and *Hsd3b6*$^{-/-}$ mice. (G, J) Representative images of corneal fluorescein staining of male (G) and female (J) mice before and after 1-h desiccation. (H, K) Pair wise comparison of corneal fluorescein staining scores of male (H) and female (K) mice. ***P* < 0.01; ****P* < 0.001, three-way ANOVA with Sidak *post hoc* test (WT male n=14; *Hsd3b6*$^{-/-}$ male n=13; WT female n=12; *Hsd3b6*$^{-/-}$ female n=18). (I, L) Measurements of tear production of male (I) and female (L) mice using phenol red-impregnated cotton threads. Values are the means ± s.e.m. (n=10 for each genotype), **P* < 0.05; ***P* < 0.01, two-tailed Student's *t* test.

NAD^+ levels determine 3β-HSD enzymatic activity.

I next explored the molecular mechanisms by which the circadian clock and aging affect the levels of 3β-HSD enzymatic activity. Interestingly, despite the fluctuating levels of 3β-HSD activity, the meibomian gland displayed a lack of daily variation in the gene expression of *Hsd3b6* (**Fig. 6A**). Western blot analysis also revealed almost constant expression of Hsd3b6 (**Fig. 6B**), indicating no apparent correlation between Hsd3b6 mRNA/protein expression and intra-tissue 3β-HSD activity. The same was also likely true for aging. Although the 3β-HSD activity declined with age (**Fig. 3A**), aging did not induce decline in the *Hsd3b6* mRNA levels (**Fig. 6C**), suggesting that other mechanisms affect 3β-HSD activity in the meibomian gland.

Nicotinamide adenine dinucleotide (NAD^+) is a key component of aging-induced disorders [35, 36]. Moreover, NAD^+ is an essential coenzyme for mediating Hsd3b6-catalyzed 3β-HSD enzymatic activity; Hsd3b6 exerts its dehydrogenase activity via converting NAD^+ to NADH. Because intracellular NAD^+ levels are known to oscillate in a circadian manner and decline with age in other peripheral tissues [37-39] I hypothesized that changes in NAD^+ levels might directly affect 3β-HSD enzymatic activity. Supporting this hypothesis, I observed that the levels of NAD^+ in the meibomian gland were decreased by approximately 50% in aged mice (**Fig. 6D**). Moreover, I directly evaluated the effect of the

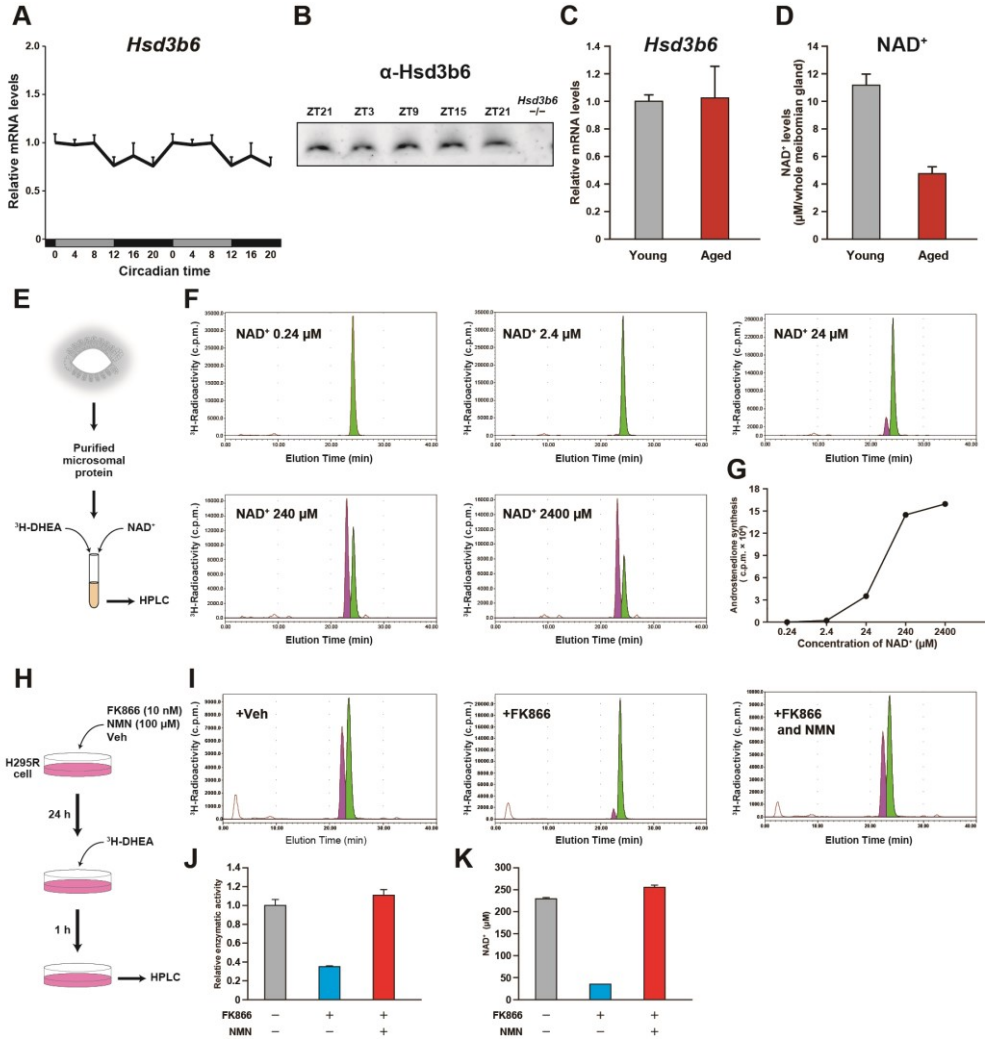

Figure 6 NAD$^+$ levels determine meibomian Hsd3b6 enzymatic activity.

(A) Circadian mRNA expression profiles of *Hsd3b6* in the meibomian glands under DD conditions. Relative expression levels were determined by qRT-PCR and normalized to those of ribosomal protein large P0 (Rplp0) gene. Data are shown in double plot. Values are means ± s.e.m. (n=4 for each data point) relative to the peak time point. (B) Temporal variations of protein expression of Hsd3b6 in the meibomian glands of WT mice in LD. Immunoreactivities seen in WT mice were completely abolished in *Hsd3b6*$^{-/-}$ mice. (C) The mRNA levels of *Hsd3b6* in the meibomian gland of young (13 weeks old) and aged (76 weeks old) mice. Relative expression levels were determined by qRT-PCR and normalized to those of ribosomal protein large P0 (Rplp0) gene. Values are the means ± s.e.m. (young, n=4; aged, n=4) relative to the value of young. (D) NAD$^+$ levels in the meibomian gland of young (28–48 weeks old) and aged (92–100 weeks old) female mice. The meibomian glands in the eyelid were isolated by laser microdissection and subjected to NAD$^+$ quantification by LC-MS/MS. Values are the means ± s.e.m. (young, n=8; aged, n=4). (E) Experimental scheme for the measurement of 3β-HSD activity *in vitro*. (F) Chromatograms showing NAD$^+$-dependent 3β-HSD enzymatic activity. The meibomian gland microsomal fraction was incubated *in vitro* with increasing doses of NAD$^+$ (0.24–2400 μM). (G) 3β-HSD enzymatic activities were determined by measuring the conversion of ^{3}H-DHEA (green) to ^{3}H-androstenedione (magenta) of D. (H) Experimental scheme for the measurement of 3β-HSD activity with cultured H295R cells. (I) Chromatograms showing NAD$^+$-dependent 3β-HSD enzymatic activity in H295R cells. Cells were incubated with FK866 (10 nM) either alone or in combination with NMN (100 μM) for 24 h prior to 3β-HSD assay. (J) 3β-HSD enzymatic activities were determined by measuring the conversion of ^{3}H-DHEA (green) to ^{3}H-androstenedione (magenta) of E. Values are the means ± s.e.m. (n=3). (K) Intracellular NAD$^+$ levels in H295R cells 24 h after treatment with FK866 (10 nM) either alone or in combination with NMN (100 μM). Values are the means ± s.e.m. (n=3).

concentration of NAD^+ on the enzymatic 3β-HSD activity *in vitro*. To this end, microsomal protein fractions containing Hsd3b6 were prepared from the meibomian gland and incubated with ^{3}H-labeled DHEA together with differing concentrations of NAD^+ (0.24–2400 μM) (**Fig. 6E**). Notably, *in vitro* 3β-HSD enzymatic activity increased in a manner depending on the dose of NAD^+ (**Fig. 6F**). Importantly, 3β-HSD had Km values for NAD^+ in the range 24–240 μM, which overlaps published NAD^+ concentrations within mammalian cells (**Fig. 6G**). Thus, 3β-HSD enzymatic activity changes as a function of NAD^+ availability.

Finally, I tested whether 3β-HSD enzymatic activity depends on the intracellular NAD^+ levels. Using human adrenocortical H295R cells, which expresses *HSD3B1*, the human counterpart of the mouse *Hsd3b6*, intracellular NAD^+ levels were manipulated pharmacologically. The cells cultured with FK866, a specific inhibitor of nicotinamide phosphoribosyl-transferase (NAMPT), which is the rate-limiting enzyme in NAD^+ biosynthesis, showed a drastic reduction of the intracellular NAD^+ levels. This reduction was completely reversed by supplementation of the precursor for NAD^+ biosynthesis, nicotinamide mononucleotide (NMN) (**Fig. 6K**). Under these conditions, I directly monitored 3β-HSD activity by adding ^{3}H-DHEA to the culture medium (**Fig. 6H**). Consistent with the alteration of intracellular NAD^+ levels, 3β-HSD activity was markedly attenuated to approximately 40% by the treatment with FK866, and its

reduction was completely restored by supplementation of NMN (**Fig. 6I, J**). These results strongly suggest that the age-associated reduction in NAD^+ levels in the meibomian gland underlies the attenuation of meibomian Hsd3b6 activity with age.

Discussion

This study unveils a new aspect of circadian clock-regulated pathology: MGD. *Bmal1* knockout mice show MGD-associated disease characterized by the acinar atrophy of the meibomian gland, and this phenotype was also observed in aged mice, as was reported in elderly humans. An extensive search for the pathogenic factor underlying the MGD in *Bmal1* knockout and aged mice led to the identification of NAD^+-dependent steroidogenic enzyme Hsd3b6, which to my knowledge has not been previously related to the development of dry eye disease. The circadian clock governs the daily enzymatic activity of Hsd3b6 in the meibomian gland. The impediment of the circadian clock could therefore be coupled to the development of MGD through the abnormal regulation of Hsd3b6-dependent local steroid production within the meibomian gland. Furthermore, meibomian Hsd3b6 steroidogenic activity declines with age. I therefore propose that Hsd3b6 would provide a promising target for the drug discovery toward aging-related MGD (**Fig. 7**).

In humans, it is well known that the prevalence of MGD-associated dry eye disease increases with age [34], but the underlying molecular mechanism is not fully understood. Furthermore, recent epidemiological studies reported an increased prevalence of sleep disturbance in dry eye patients [40, 41]. However, the cause-and-effect relationship between sleep disturbance and ocular surface health remain elusive, and the underlying

mechanism has remained unexplored. In this study, I provided molecular and genetic evidence that the meibomian Hsd3b6 is a key enzyme that links circadian clock dysfunction and aging with the development of evaporative dry eye. Interestingly, although the mRNA of human HSD3B1, which is a functional counterpart to mouse Hsd3b6, is expressed in the meibomian gland [42], the physiological function of this enzyme in the meibomian gland remains unknown. Based on the findings in my thesis, the potential involvement of human HSD3B1 in the meibomian gland pathophysiology merits further investigation.

NAD^+ is an essential coenzyme involved in over 500 enzymatic reactions and plays key roles in the regulation of almost all major biological processes [43]. Although these roles of NAD^+ in redox reactions are well understood, NAD^+ biology has more recently gained attention following recognition that it also functions as a co-substrate for a range of different enzymes, including sirtuins (SIRTs), poly(ADP-ribose) polymerases (PARPs) and cyclic ADP-ribose synthases (CD38), where NAD^+ is actively degraded during the enzymatic processes catalyzed by these enzymes [35, 44, 45]. In particular, decreased activity of SIRTs caused by pathophysiological decline in NAD^+ biosynthesis has strongly associated with the susceptibility of organs to aging and age-related disease such as diabetes, neurodegenerative diseases, osteoporosis, and others [46-48]. In this study, I identified NAD^+-dependent steroidogenic enzyme

Hsd3b6 in the meibomian gland as a possible key component of age-associated dry eye disease.

In my study, it is unclear whether the meibomian NAD^+ levels oscillate in a circadian fashion. It is known that the abundance of hepatic NAD^+ displays circadian rhythmicity due to a direct circadian transcriptional control of the rate-limiting enzyme of NAD^+ biosynthesis, NAMPT [37-39]. Even in the conditions that SIRTs protein abundance is relatively stable, the circadian oscillation of NAD^+ could therefore drive diurnal SIRTs activities [37, 38]. Future studies are necessary to determine whether the meibomian NAD^+ levels dictate diurnal rhythm of Hsd3b6 enzymatic activity in the meibomian gland.

Because the decline in 3β-HSD enzymatic activity was restored by the supplementation of the precursor for NAD^+ synthesis (NMN) in cultured human steroidogenic cells, it is tempting to speculate that the recovery from the decrease in meibomian NAD^+ levels could ameliorate MGD. NAD^+ levels can be increased either by promoting its synthesis, by enhancing the enzymes involved in NAD^+ biosynthesis or administration of NAD^+ precursor molecules, or by limiting its consumption. Among them, two key NAD^+ intermediates, NMN and nicotinamide riboside (NR), have been extensively studied over the past several years [36]. NAD^+ salvage pathway is the key pathway for maintaining cellular NAD^+ levels. The NAD^+-consuming enzymes (SIRTs, PARPs, and CD38) generate

nicotinamide (NAM) as a by-product of their enzymatic activities, and NAMPT recycles NAM to NMN, which is converted into NAD^+ by nicotinamide mononucleotide adenylyltransferase (NMNAT). The precursor NR is directed into the salvage pathway, bypassing the need for the rate-limiting enzyme NAMPT in the salvage pathway. Recently it has been shown that supplementing these NAD^+ intermediates has indeed preventive and therapeutic effects, ameliorating age-associated pathophysiologies and disease conditions [35, 36, 49, 50]. Therefore, it will be worth testing whether the supplementation of NAD^+ intermediates could ameliorate MGD through the restoration of Hsd3b6 enzymatic activity in the meibomian gland.

3β-HSD enzyme family is essential for the production of active steroid hormones not only in the meibomian gland, but also in other steroidogenic tissues such as the adrenal gland, testis, ovary, skin, and placenta. In the classical steroidogenic tissues, it is well known that not only androgen and estrogen but also aldosterone levels decrease with age in many species, including humans and mice [51, 52]. Therefore, my finding that the attenuation of NAD^+-dependent 3β-HSD activity with age underlies the abnormal steroidogenesis in the meibomian gland could further apply to the mechanism(s) behind aging-associated steroidogenic disorders in various steroid-producing tissues.

In summary, I revealed that the meibomian gland possesses robust

circadian clock system that regulates meibomian NAD^+-dependent steroidogenic enzyme Hsd3b6 activity. Meibomian intrinsic Hsd3b6 activity contributes to local steroid production in the meibomian glands and maintains their morphology. Moreover, I have found MGD in circadian clock-deficient *Bmal1* knockout and aged mice. The inactivation of Hsd3b6 activity induces the loss of local steroidogenesis in the meibomian gland and as a consequence leads to the development of MGD and MGD-associated dry eye disease. Circadian malfunction and aging both induce reduction of NAD^+-dependent enzymatic activity of Hsd3b6. My data therefore propose that Hsd3b6 might be a promising target for the drug discovery of dry eye disease.

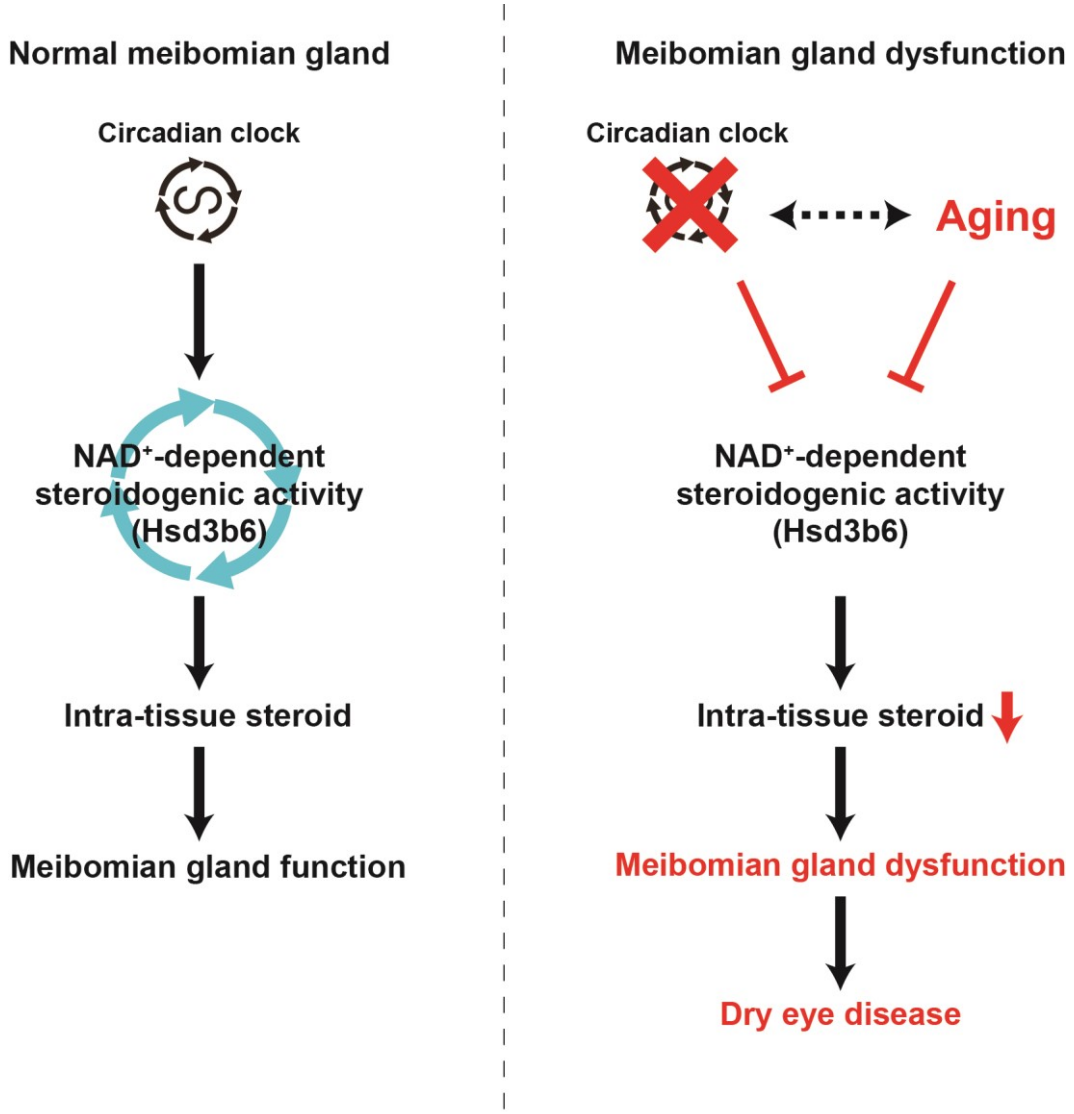

Figure 7 Schematic model showing the regulation of Hsd3b6 enzymatic activity in the meibomian glands.
In the normal meibomian gland, NAD^+-dependent steroidogenic activity of Hsd3b6 is regulated by circadian clock and maintains meibomian gland function (left). Crcadian clock malfunction and aging both lead to reduction of NAD^+-dependent enzymatic activity of Hsd3b6, which reduces intra-tissue testosterone and leads to MGD-associated evaporative dry eye disease (right).

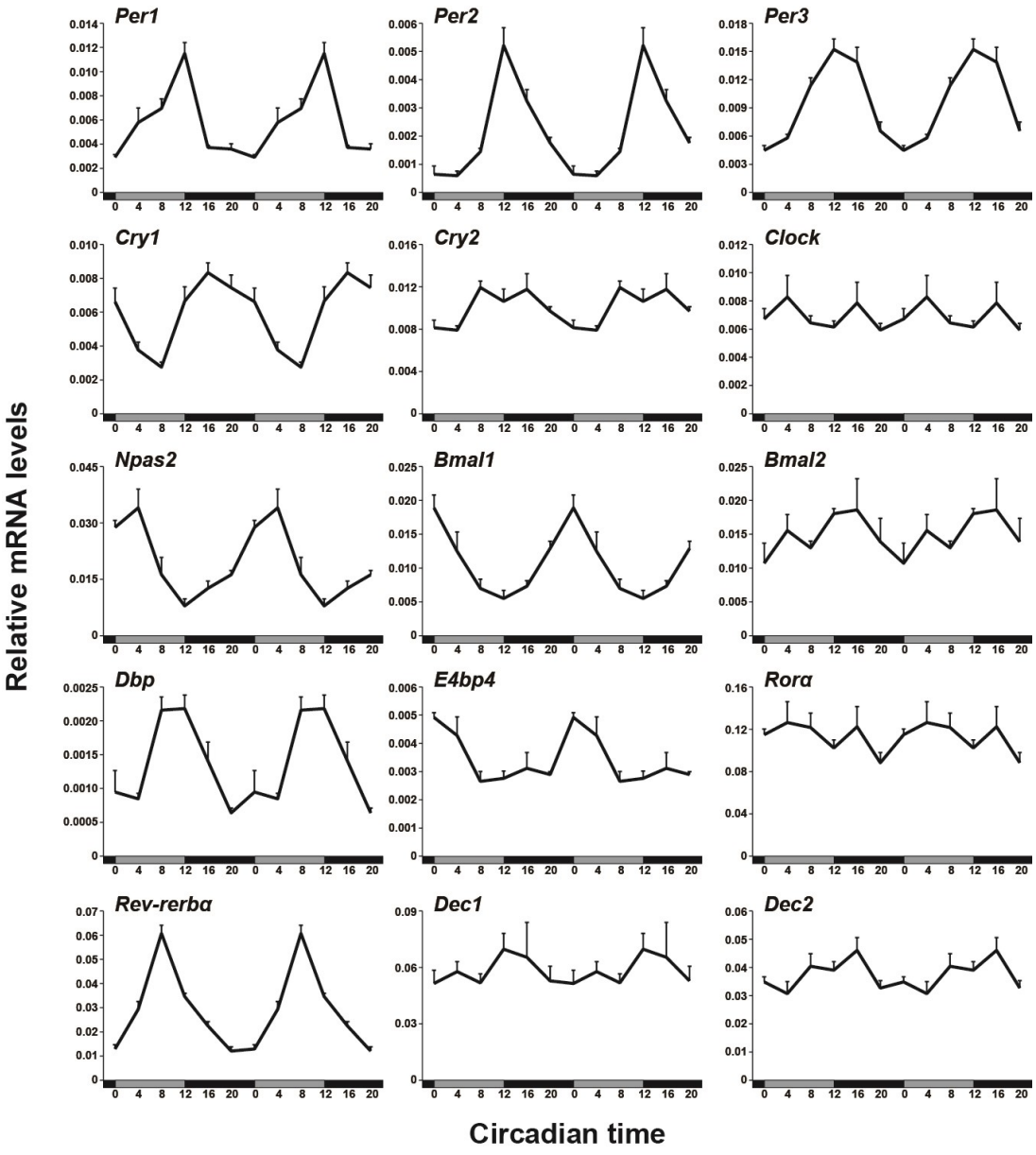

Supplementary Figure 1 Expression of circadian clock genes in the meibomian glands.

Circadian expression profiles of 15 clock genes in the meibomian glands under DD conditions. Relative expression levels were determined by qRT-PCR using a Fluidigm chip and normalized to those of ribosomal protein large P0 (Rplp0) gene. Data were double plotted. Values are the means ± s.e.m. (n=4 for each data point).

References

1. Panda, S. (2016). Circadian physiology of metabolism. Science *354*, 1008-1015.
2. Takahashi, J.S. (2017). Transcriptional architecture of the mammalian circadian clock. Nat Rev Genet *18*, 164-179.
3. Wijnen, H., and Young, M.W. (2006). Interplay of circadian clocks and metabolic rhythms. Annu. Rev. Genet. *40*, 409-448.
4. Doi, M., Takahashi, Y., Komatsu, R., Yamazaki, F., Yamada, H., Haraguchi, S., Emoto, N., Okuno, Y., Tsujimoto, G., Kanematsu, A., et al. (2010). Salt-sensitive hypertension in circadian clock-deficient Cry-null mice involves dysregulated adrenal Hsd3b6. Nat Med *16*, 67-74.
5. Logan, R.W., and McClung, C.A. (2019). Rhythms of life: circadian disruption and brain disorders across the lifespan. Nat Rev Neurosci *20*, 49-65.
6. Takahashi, J.S., Hong, H.K., Ko, C.H., and McDearmon, E.L. (2008). The genetics of mammalian circadian order and disorder: implications for physiology and disease. Nat Rev Genet *9*, 764-775.
7. Tong, L., Chaurasia, S.S., Mehta, J.S., and Beuerman, R.W. (2010). Screening for meibomian gland disease: its relation to dry eye subtypes and symptoms in a tertiary referral clinic in singapore. Invest Ophthalmol Vis Sci *51*, 3449-3454.

8. Viso, E., Gude, F., and Rodriguez-Ares, M.T. (2011). The association of meibomian gland dysfunction and other common ocular diseases with dry eye: a population-based study in Spain. Cornea *30*, 1-6.

9. Farrand, K.F., Fridman, M., Stillman, I.O., and Schaumberg, D.A. (2017). Prevalence of Diagnosed Dry Eye Disease in the United States Among Adults Aged 18 Years and Older. Am. J. Ophthalmol. *182*, 90-98.

10. Moss, S.E., Klein, R., and Klein, B.E. (2000). Prevalence of and risk factors for dry eye syndrome. Arch Ophthalmol *118*, 1264-1268.

11. Nichols, J.J., Ziegler, C., Mitchell, G.L., and Nichols, K.K. (2005). Self-reported dry eye disease across refractive modalities. Invest Ophthalmol Vis Sci *46*, 1911-1914.

12. Sullivan, D.A., Rocha, E.M., Aragona, P., Clayton, J.A., Ding, J., Golebiowski, B., Hampel, U., McDermott, A.M., Schaumberg, D.A., Srinivasan, S., et al. (2017). TFOS DEWS II Sex, Gender, and Hormones Report. Ocul Surf *15*, 284-333.

13. Truong, S., Cole, N., Stapleton, F., and Golebiowski, B. (2014). Sex hormones and the dry eye. Clin Exp Optom *97*, 324-336.

14. Khandelwal, P., Liu, S., and Sullivan, D.A. (2012). Androgen regulation of gene expression in human meibomian gland and conjunctival epithelial cells. Mol Vis *18*, 1055-1067.

15. Sullivan, D.A., Sullivan, B.D., Evans, J.E., Schirra, F., Yamagami, H., Liu, M., Richards, S.M., Suzuki, T., Schaumberg, D.A., Sullivan, R.M., et al. (2002). Androgen deficiency, Meibomian gland dysfunction, and evaporative dry eye. Ann. N. Y. Acad. Sci. *966*, 211-222.

16. Sullivan, D.A., Sullivan, B.D., Ullman, M.D., Rocha, E.M., Krenzer, K.L., Cermak, J.M., Toda, I., Doane, M.G., Evans, J.E., and Wickham, L.A. (2000). Androgen influence on the meibomian gland. Invest Ophthalmol Vis Sci *41*, 3732-3742.

17. Knop, E., Knop, N., Millar, T., Obata, H., and Sullivan, D.A. (2011). The international workshop on meibomian gland dysfunction: report of the subcommittee on anatomy, physiology, and pathophysiology of the meibomian gland. Invest Ophthalmol Vis Sci *52*, 1938-1978.

18. Schaumberg, D.A., Nichols, J.J., Papas, E.B., Tong, L., Uchino, M., and Nichols, K.K. (2011). The international workshop on meibomian gland dysfunction: report of the subcommittee on the epidemiology of, and associated risk factors for, MGD. Invest Ophthalmol Vis Sci *52*, 1994-2005.

19. Miller, W.L., and Auchus, R.J. (2011). The molecular biology, biochemistry, and physiology of human steroidogenesis and its disorders. Endocr. Rev. *32*, 81-151.

20. Yagi, T., Tokunaga, T., Furuta, Y., Nada, S., Yoshida, M., Tsukada,

T., Saga, Y., Takeda, N., Ikawa, Y., and Aizawa, S. (1993). A novel ES cell line, TT2, with high germline-differentiating potency. Anal. Biochem. *214*, 70-76.

21. Shimba, S., Ogawa, T., Hitosugi, S., Ichihashi, Y., Nakadaira, Y., Kobayashi, M., Tezuka, M., Kosuge, Y., Ishige, K., Ito, Y., et al. (2011). Deficient of a clock gene, brain and muscle Arnt-like protein-1 (BMAL1), induces dyslipidemia and ectopic fat formation. PLoS One *6*, e25231.

22. JA, B. (1940). A simple technic for toto staining of tarsal and sebaceous glands. Stain Technol *15*, 29-30.

23. Lee, H., Kim, C.E., Ahn, B.N., and Yang, J. (2017). Anti-inflammatory effect of hydroxyproline-GQDGLAGPK in desiccation stress-induced experimental dry eye mouse. Sci Rep *7*, 7413.

24. Hamano, H., Hori, M., Hamano, T., Mitsunaga, S., Maeshima, J., Kojima, S., and Kawabe, H. (1983). A new method for measuring tears. Clao J *9*, 281-289.

25. Tanaka, R., Tainaka, M., Ota, T., Mizuguchi, N., Kato, H., Urabe, S., Chen, Y., Fustin, J.M., Yamaguchi, Y., Doi, M., et al. (2011). Accurate determination of S-phase fraction in proliferative cells by dual fluorescence and peroxidase immunohistochemistry with 5-bromo-2'-deoxyuridine (BrdU) and Ki67 antibodies. J Histochem

Cytochem *59*, 791-798.

26. Yamamura, K., Doi, M., Hayashi, H., Ota, T., Murai, I., Hotta, Y., Komatsu, R., and Okamura, H. (2014). Immunolocalization of murine type VI 3beta-hydroxysteroid dehydrogenase in the adrenal gland, testis, skin, and placenta. Mol. Cell. Endocrinol. *382*, 131-138.

27. Yoshino, J., and Imai, S. (2013). Accurate measurement of nicotinamide adenine dinucleotide (NAD(+)) with high-performance liquid chromatography. Methods Mol Biol *1077*, 203-215.

28. Doi, M., Murai, I., Kunisue, S., Setsu, G., Uchio, N., Tanaka, R., Kobayashi, S., Shimatani, H., Hayashi, H., Chao, H., et al. (2016). Gpr176 is a Gz-linked orphan G-protein coupled receptor that sets the pace of circadian behavior. Nat. Commun. *in press*.

29. Tainaka, M., Doi, M., Inoue, Y., Murai, I., and Okamura, H. (2018). Circadian PER2 protein oscillations do not persist in cycloheximide-treated mouse embryonic fibroblasts in culture. Chronobiol. Int. *35*, 132-136.

30. Hughes, M.E., Hogenesch, J.B., and Kornacker, K. (2010). JTK_CYCLE: an efficient nonparametric algorithm for detecting rhythmic components in genome-scale data sets. J. Biol. Rhythms *25*, 372-380.

31. Yang, X., Downes, M., Yu, R.T., Bookout, A.L., He, W., Straume,

M., Mangelsdorf, D.J., and Evans, R.M. (2006). Nuclear receptor expression links the circadian clock to metabolism. Cell *126*, 801-810.

32. Simard, J., Ricketts, M.L., Gingras, S., Soucy, P., Feltus, F.A., and Melner, M.H. (2005). Molecular biology of the 3beta-hydroxysteroid dehydrogenase/delta5-delta4 isomerase gene family. Endocr. Rev. *26*, 525-582.

33. Kondratov, R.V., Kondratova, A.A., Gorbacheva, V.Y., Vykhovanets, O.V., and Antoch, M.P. (2006). Early aging and age-related pathologies in mice deficient in BMAL1, the core componentof the circadian clock. Genes Dev. *20*, 1868-1873.

34. Arita, R., Itoh, K., Inoue, K., and Amano, S. (2008). Noncontact infrared meibography to document age-related changes of the meibomian glands in a normal population. Ophthalmology *115*, 911-915.

35. Rajman, L., Chwalek, K., and Sinclair, D.A. (2018). Therapeutic Potential of NAD-Boosting Molecules: The In Vivo Evidence. Cell Metab *27*, 529-547.

36. Yoshino, J., Baur, J.A., and Imai, S.I. (2018). NAD(+) Intermediates: The Biology and Therapeutic Potential of NMN and NR. Cell Metab *27*, 513-528.

37. Nakahata, Y., Sahar, S., Astarita, G., Kaluzova, M., and

Sassone-Corsi, P. (2009). Circadian control of the NAD+ salvage pathway by CLOCK-SIRT1. Science *324*, 654-657.

38. Peek, C.B., Affinati, A.H., Ramsey, K.M., Kuo, H.Y., Yu, W., Sena, L.A., Ilkayeva, O., Marcheva, B., Kobayashi, Y., Omura, C., et al. (2013). Circadian clock NAD+ cycle drives mitochondrial oxidative metabolism in mice. Science *342*, 1243417.

39. Ramsey, K.M., Yoshino, J., Brace, C.S., Abrassart, D., Kobayashi, Y., Marcheva, B., Hong, H.K., Chong, J.L., Buhr, E.D., Lee, C., et al. (2009). Circadian clock feedback cycle through NAMPT-mediated NAD+ biosynthesis. Science *324*, 651-654.

40. Ayaki, M., Kawashima, M., Negishi, K., Kishimoto, T., Mimura, M., and Tsubota, K. (2016). Sleep and mood disorders in dry eye disease and allied irritating ocular diseases. Sci Rep *6*, 22480.

41. Ayaki, M., Kawashima, M., Negishi, K., and Tsubota, K. (2015). High prevalence of sleep and mood disorders in dry eye patients: survey of 1,000 eye clinic visitors. Neuropsychiatr Dis Treat *11*, 889-894.

42. Schirra, F., Suzuki, T., Dickinson, D.P., Townsend, D.J., Gipson, I.K., and Sullivan, D.A. (2006). Identification of steroidogenic enzyme mRNAs in the human lacrimal gland, meibomian gland, cornea, and conjunctiva. Cornea *25*, 438-442.

43. Ansari, H.R., and Raghava, G.P. (2010). Identification of NAD

interacting residues in proteins. BMC Bioinformatics *11*, 160.

44. Chini, C.C.S., Tarrago, M.G., and Chini, E.N. (2017). NAD and the aging process: Role in life, death and everything in between. Mol. Cell. Endocrinol. *455*, 62-74.

45. Katsyuba, E., and Auwerx, J. (2017). Modulating NAD(+) metabolism, from bench to bedside. Embo J *36*, 2670-2683.

46. Chang, H.C., and Guarente, L. (2014). SIRT1 and other sirtuins in metabolism. Trends Endocrinol Metab *25*, 138-145.

47. Guarente, L. (2013). Calorie restriction and sirtuins revisited. Genes Dev. *27*, 2072-2085.

48. Imai, S., and Guarente, L. (2014). NAD+ and sirtuins in aging and disease. Trends Cell Biol. *24*, 464-471.

49. Fang, E.F., Lautrup, S., Hou, Y., Demarest, T.G., Croteau, D.L., Mattson, M.P., and Bohr, V.A. (2017). NAD(+) in Aging: Molecular Mechanisms and Translational Implications. Trends Mol. Med. *23*, 899-916.

50. Verdin, E. (2015). NAD(+) in aging, metabolism, and neurodegeneration. Science *350*, 1208-1213.

51. Ishikawa, S., Saito, T., Fukagawa, A., Higashiyama, M., Nakamura, T., Kusaka, I., Nagasaka, S., and Honda, K. (2001). Close association of urinary excretion of aquaporin-2 with appropriate and inappropriate arginine vasopressin-dependent antidiuresis in

hyponatremia in elderly subjects. J Clin Endocrinol Metab *86*, 1665-1671.

52. Labrie, F., Belanger, A., Cusan, L., Gomez, J.L., and Candas, B. (1997). Marked decline in serum concentrations of adrenal C19 sex steroid precursors and conjugated androgen metabolites during aging. J Clin Endocrinol Metab *82*, 2396-2402.

Acknowledgement

I would first like to express my appreciation for the crucial role of to my thesis Prof. Masao Doi and Prof. Hitoshi Okamura, who encouraged me to pursue my research interest through valuable advice and discussion.

I would also like to appreciate Prof. Hideaki Kakeya and Dr. Kensuke Kaneko (Kyoto Univ.) for supporting the analysis of LC-MS/MS. I would like to express my gratitude to Yuki Sugiura (Keio Univ.) for MALDI-imaging MS analysis. Moreover, I thank to Dr. Shogo Haraguchi (Showa Univ.) for helping the quantification of testosterone by LC-MS/MS. My sincere thanks also goes to Prof. Hozumi Motohashi (Tohoku Univ.) who provided me aged mice.

I am grateful to Dr. Takumi Ota, Mrs. Yuki Nakagawa, Mr. Hiroki Nakamura, and Ms. Aya Shimada for the technical assistance and contributions.

Finally, I would like to thank my family: my parents and to my sister for supporting me spiritually throughout writing this thesis and my life in general.